A high-resolution, spatially explicit estimate of fossil-fuel CO2 emissions from the Tokyo Metropolis, Japan

Richao Cong (richao.cong@nies.go.jp)
National Institute for Environmental Studies https://orcid.org/0000-0002-6315-6147
Makoto Saito
National Institute for Environmental Studies
Tetsuo Fukui
Institute of Behavioral Sciences
Ryuichi Hirata
National Institute for Environmental Studies
Akihiko Ito
National Institute for Environmental Studies

Methodology

Keywords: Carbon dioxide, CO2 emission inventory, Fossil fuel, GIS, High-resolution map, Tokyo emissions

Posted Date: January 7th, 2021

DOI: https://doi.org/10.21203/rs.3.rs-17565/v4

A high-resolution, spatially explicit estimate of fossil-fuel CO_2 emissions from the Tokyo Metropolis, Japan

Richao Cong[1,2*], Makoto Saito[1*], Tetsuo Fukui[3], Ryuichi Hirata[1] and Akihiko Ito[1]

[1] Center for Global Environmental Research, National Institute for Environmental Studies, Tsukuba, Japan

[2] Fukushima Branch, National Institute for Environmental Studies, Tamura District, Japan

[3] Institute of Behavioral Sciences, Tokyo, Japan

**Correspondence*:

richao.cong@nies.go.jp; saito.makoto@nies.go.jp

Abstract

Background: The quantification of urban greenhouse gas (GHG) emissions is an important task in combating climate change. Emission inventories that include spatially explicit emission estimates facilitate the accurate tracking of emission changes, identification of emission sources, and formulation of policies for climate-change mitigation. Many currently available gridded emission estimates are based on the disaggregation of country- or state-wide emission estimates, which may be useful in describing city-wide emissions but are of limited value in tracking changes at subnational levels. Urban GHG emissions should therefore be quantified with a true bottom-up approach.

Results: Multi-resolution, spatially explicit estimates of fossil-fuel carbon dioxide ($FFCO_2$) emissions from the Tokyo Metropolis, Japan, were derived. Spatially explicit emission data were collected for point (e.g., power plants and waste incinerators), line (mostly traffic), and area (e.g., residential and commercial areas) sources. Emissions were mapped on the basis of emission rates calculated for source locations. Activity, emissions, and spatial data were integrated, and the results were visualized using a geographic information system approach.

Conclusions: The annual total $FFCO_2$ emissions from the Tokyo Metropolis in 2014 were 43,916 Gg CO_2, with the road-transportation sector (16,323 Gg CO_2) accounting for 37.2% of the total. Spatial emission patterns were verified via a comparison with the East Asian Air Pollutant Emission Grid Database for Japan (EAGrid-Japan) and the Open-source Data Inventory for Anthropogenic CO_2 (ODIAC), which demonstrated the applicability of this methodology to other prefectures and therefore the entire country.

Keywords: Carbon dioxide, CO_2 emission inventory, Fossil fuel, GIS, High-resolution map, Tokyo emissions

Background

Fossil-fuel combustion is a major contributor to increasing atmospheric carbon dioxide (CO_2) concentrations [1], with cities worldwide being responsible for more than 70% of the global total fossil-fuel CO_2 emissions ($FFCO_2$) [2]. As large sources of $FFCO_2$, cities have great potential for emission mitigation [3]. In response to the need for local climate action, many global cities have participated in climate action groups, such as the C40 Cities Climate Leadership Group [4] and the Global Covenant of Mayors for Climate & Energy [5], and started compiling emission inventories (EIs). The EIs are often compiled following the Global Protocol for Community-Scale Greenhouse Gas Emission Inventories (GPC) [6]. The Paris Agreement of the United Nations Framework Convention on Climate Change (UNFCCC) recognizes the importance of climate-change mitigation at subnational levels [7]. However, subnational emission estimates (e.g., state, province, city (UN-Habitat [2]), and private sector) are beyond the scope of the current Intergovernmental Panel on Climate Change (IPCC) guidelines. The inventory framework implemented under the Kyoto Protocol focuses on national compliance with global emission-reduction targets [8], rather than monitoring emission changes at subnational levels.

Cities play an important role for implementation of climate-remediation actions. Previous studies have accounted for city emissions using various approaches, including the purely geographic-based (PB) [9, 10], consumption-based carbon-footprint [11, 12], and community-wide infrastructure-footprint [13, 14] approaches. Such studies estimate emissions for whole cities by monitoring activities at the city level. Due to recent mitigation action, the need for more detailed information on temporospatial distributions of emissions has increased, necessitating the assessment of emission changes at sub-city levels.

For spatially explicit emission data, Gurney et al. [15] loosely categorized emission modeling approaches as 'downscaled' or 'bottom-up'. The downscaled approach is used mainly for global-scale greenhouse gas (GHG) EIs, and downscales national total emissions to source-related proxies [16, 17, 18]. Conversely, the bottom-up approach estimates temporospatially explicit emissions based on sectoral activity data derived from socioeconomic sources. These two approaches result in large discrepancies in urban-scale $FFCO_2$ emissions, due to the limitations of downscaled EIs in capturing spatial patterns of complex source activities [19]. Since the bottom-up approach considers local-scale emission sources, emission estimates based on this approach are likely suitable for tracking emission changes in sub-city and local areas. For example, the Hestia Project developed multi-resolution emission data for four US cities using a bottom-up approach [20-23]. These EIs provide bottom-up $FFCO_2$ emission data for the urban domain with building/street and hourly temporospatial resolution. GHG emissions for Poland and Ukraine were estimated based on geoinformation technologies, where emissions were determined at source locations (points, lines, and areas), taking into account emission processes [24]. This approach enables the tracking of changes in local emissions, allowing the evaluation of existing EIs over the domain of a single country [24, 25]. Limited by the availability of fossil fuel use from individual sources, previous studies succeeded in disaggregating the reported CO_2 annual emissions/fuel use from a larger scale e.g., county/provincial level to individual sources/proxies for temporospatially explicit estimates (Table1). This study also uses disaggregating processes for area-sources, however, the annual emissions by point and line sources are directly estimated for individual sources/proxies without disaggregation, by integrating spatially-explicit statistics data with region-specific secondary-derived emission factors.

This study presents a detailed framework for the direct accounting of local $FFCO_2$ emissions in Japan using a bottom-up approach (i.e., PB approach for direct emissions (Scope-1) [6]) and demonstrates its application to multi-resolution emissions at point, road, building, or mesh levels. As a pilot study, we first consider spatially explicit $FFCO_2$ emission data for the Tokyo Metropolis (population 13.6 M in 2016; area 2,189 km^2) for the year 2014. This study is distinguished from the East Asian Air Pollutant Emission Grid Database for Japan (EAGrid-Japan) by the use of a multi-resolution approach and updated information. Here, we describe the various statistical and geospatial data used in estimating and mapping emissions, compare our emission estimates with existing estimates at aggregated city and grid cell levels, and discuss current limitations and future improvements.

Methods

Emission definition and modeling framework

The focus here is on quantifying $FFCO_2$ emissions from the Tokyo Metropolis using the modeling framework described in Fig. 1. Following previous studies [20, 24, 32], a multi-resolution emission modeling approach was employed, where CO_2 emissions ('emissions' hereinafter) were calculated on an individual source basis in a bottom-up manner, rather than using aggregated emission-sector levels. Emissions were spatially allocated using verified geographic latitude and longitude coordinates (mainly for point sources) and spatial geolocation data (for line and area sources), with examples of point-source locations and geospatial data shown in Fig. 2.

The total emissions for the year 2014 were calculated using the best available locally collected data following the 2006 IPCC guidelines [33]. Emission sources therefore included electricity generation (IPCC code 1A1ai), civil aviation (1A3a), waterborne navigation (1A3d), waste incineration (4C1), road transportation (1A3bi, 1A3bii, and 1A3biii), industrial and commercial sources (1A1aiii, 1A2, 1A4a, and 1A4ciii), residential sources (1A4b), and agricultural machine use (1A4cii). These emissions were calculated using the Tier 3 approach [33]. The emission-sector definitions, spatial information and data, activity data, and emission factors are summarized in Table 2.

Point-source emissions

Point-source emissions include those from electricity generation, civil aviation, waterborne navigation, and waste incineration (Table 2). For electricity generation, only fossil-fueled power plants in Tokyo (n = 19) were considered (see Additional File 1; Table S1 for details). The 2014 total emissions from all power plants were calculated by formula:

$$E_{eg} = 24 \cdot \sum_{i=1}^{n} \sum_{j=1}^{12} C_i \cdot D_j \cdot R_{g,j} \cdot EF_{g,j}, \quad (1)$$

where E_{eg} represents the total annual emissions from electricity generation (Gg CO_2); the coefficient 24 indicates the number of hours per day; C_i is the electricity generation capacity (kW) of power plant i in Tokyo with one type of generator (steam, gas cogeneration, or internal combustion); D_j is the number of days in month j; $R_{g,j}$ is the mean utilization efficiency of fossil-fueled power plants with generator type g in month j for 2014; and $EF_{g,j}$ is the emission factor for fossil-fueled electricity generation by generator type g in month j (Gg CO_2 kWh^{-1}). The C_i values were obtained from the Electrical Japan Database (data were collected in April 2017) [34] and operator companies [35–37]. The $R_{g,j}$ values are reported by power plant operators and published by the government of Japan each year [38]. The emission factors of power plants in 2014 ($EF_{g,j}$) were derived from electricity generation amounts by power plants, the monthly fuel consumption (e.g., coal, crude oil, heavy oil, light oil, liquefied natural gas, liquefied petroleum gas, and other gas) [39], and official guidelines for GHG emissions counting [40]. Where there was a lack of individual data for a plant, R_j and EF_j values for plants with the same type of generator were used. The stack centroid was used as the representative emission location for multiple smoke stacks in a single power plant facility. An example of point-source emissions in SG Ward (see Table S2) is shown in Fig. 2A.

Civil aviation emissions included those from passenger and cargo aircraft during landing and take-off (LTO) at an international airport, four helipads, and six domestic airports (Table S1). The 2014 total emissions from LTO movements were calculated as follows:

$$E_{ca} = \sum_{i=1}^{n} \sum_{a} F_{a,i} \cdot N_a \cdot EC_e \cdot EF_f, \quad (2)$$

where E_{ca} represents the total annual emissions from civil aviation (Gg CO_2); $F_{a,i}$ is the total number of arrivals for type a aircraft with one type of engine at airport i in 2014; N_a is the number of engines on type a aircraft; EC_e is the jet fuel ('energy') consumption per engine during an LTO cycle by engine type e (Gg per engine per LTO); and EF_f is the emission factor of jet fuel (3.154 Gg CO_2 Gg^{-1}) [40]. The $F_{a,i}$ and N_a values were summarized from 2014 flight records [41–49] and websites [50]. The monthly proportion of aircraft types at Haneda airport was used as the annual proportion for 2014 due to the lack of annual flight timetables for each aircraft type. The monthly proportions of arrivals for each aircraft type were obtained from flight timetables for April 2017 [51, 52]. The EC_e values were extracted from the Aircraft Engine Emissions Databank of the International Civil Aviation Organization (ICAO) [53] and guidance on helicopter emissions [33, 54]. As aircraft are mobile sources, the calculated emissions were mapped using representative points on airport runways (diameter ~1 km) as point sources.

Emissions from the waterborne navigation sector included emissions from fuel consumed by vessels during round trips to ports in Tokyo (n = 15; Table S1). The 2014 total emissions from vessels were calculated as follows:

$$E_{wn} = \sum_{i=1}^{n} \sum_{t,m} I_{t,m} \cdot R_{t,m} \cdot T_{t,m} \cdot N_{t,i} \cdot EF_t, \quad (3)$$

where E_{wn} represents the total annual emissions by vessels (Gg CO_2); $I_{t,m}$ is the emission intensity of fuels (tonne per vessel) for type t vessels (including merchant vessels, car ferries, evacuation vessels, fishing vessels, and other vessels) at mode m (travelling, cargo loading and unloading, and mooring); $R_{t,m}$ is the load factor of type-t vessels in mode m; $T_{t,m}$ is the fuel consumption time of type-t vessels in mode m (h); $N_{t,i}$ is the annual number of type-t vessels travelling to port i; and EF_t is the emission factor (Gg CO_2 $tonne^{-1}$) for type-t vessels consuming heavy oil or light oil. The $I_{t,m}$, $R_{t,m}$, and $T_{t,m}$ values and the average travel speed for these vessels were obtained from technical reports [55, 56]. As shown by the parameters listed in Table S3, the mean travel distance was assumed to be 1 km in travelling mode to derive the travel time. The emissions from travelling mode were considered for fishing vessels but all mode were considered for the other types of vessels. The $N_{t,i}$ values were obtained from statistical data on vessels in ports [57, 58]. The EF_t data were extracted from the official guideline [40]. As waterborne vessels are mobile sources, representative points on port buildings were used as their point-source locations.

Emissions from incineration plants do not contribute to $FFCO_2$ emissions. However, this study included their emissions because the emission intensity is significant. Emissions from incineration plants for municipal solid waste (MSW, n = 46) and industrial waste (n = 15) (Table S1) included those from the combustion of wastes containing carbon (e.g., papers, plastics, textiles, rubbers, and oil) and the combustion agent (CA, "city gas" comprising liquid petroleum gas and natural gas). Emissions from MSW waste combustion were calculated as follows:

$$E_{mw} = \sum_{i=1}^{n} (\sum_{c} T_i \cdot R_{c,i} \cdot FC \cdot EF_c + T_i \cdot CR \cdot EF), \quad (4)$$

where E_{mw} represents the 2014 total emissions from MSW incineration (Gg CO_2); T_i is the total amount of combustible content in waste (tonne) incinerated annually at plant i; $R_{c,i}$ is the proportion of type-c content of waste (i.e., waste paper, plastic, rubber, and textiles in MSW) at plant i; FC is the fossil carbon content in waste; EF_c is the emission factor for combustible content type c in waste (paper 1.69×10^{-5}; plastic 2.55×10^{-3}; textiles 2.29×10^{-3}; rubber 1.72×10^{-3} Gg CO_2 tonne^{-1}) [40]; CR is the mean consumption of CA (1.29 m^3 tonne^{-1}) [59]; and EF is the emission factor for CA (2.21×10^{-6} Gg CO_2 m^{-3}) [40]. The T_i and $R_{c,i}$ values for all 46 MSW incineration plants in Tokyo were obtained from the investigation report on MSW for Tokyo, 2014 [60]. Here we assumed that paper and textiles in wastes were in equal amounts and the fossil carbon content (FC) of these wastes were 50%. The CR values derived from available data for 19 MSW incineration plants in Tokyo [59] were used for all MSW incineration plants.

Emissions from industrial waste combustion were calculated as follows:

$$E_{iw} = \sum_c T_c \cdot FC \cdot EF_c, \quad (5)$$

where E_{iw} represents the 2014 total emissions from industrial waste incineration (Gg CO_2); T_c is the total annual amount of combustible content in waste (tonnes) at all plants in Tokyo for type c (i.e., waste paper, plastic, textiles, and oil in industrial waste); and EF_c is the emission factor for fossil carbon in waste type c (oil 2.92×10^{-3} Gg CO_2 tonne^{-1}) [40]. T_c values were extracted from the investigation report on industrial waste incineration [61]. The FC value for industrial waste was assumed to be 1 with no CA used due to the high-purity carbon content. The emissions from 15 industrial-waste incineration plants were derived by allocating the E_{iw} with plant disposal capacities [62]. The central points of the chimneys at waste incineration plants were mapped as emission points.

Line-source emissions

Line-source emissions included those of the road-transport sector, based on traffic census data compiled by the Ministry of Land, Infrastructure, Transport and Tourism for each prefecture every five years, with the latest being in 2015 [63]. The census data include road information (name, width, length, number of lanes, and classification for each road segment), hourly and daily traffic volumes, and 12-h mean daytime vehicle speeds for small vehicles (light passenger cars, regular passenger cars, light trucks, and small freight cars) and large vehicles (bus, regular truck, and special-use vehicles). The road segment data indicate the network links, as shown in the example of a digital road map (DRM; [64]) in Fig. 2B. The census targets five road classifications: high-speed national highways, urban highways, general national highways, major regional roads (prefectural roads and designated city roads), and general regional roads. Emissions on minor roads that were not covered by the census were not considered.

Road transportation emissions were calculated for single road segments (n = 45,564) as follows:

$$E_{rt} = \sum_{i=1}^{n} \sum_v Q_{v,i} \cdot L_i \cdot EF_{v,s}, \quad (6)$$

where E_{rt} represents the 2014 total emissions from road transportation (Gg CO_2); $Q_{v,i}$ is the annual traffic volume (derived from daily data) for type v vehicles at a vehicle speed (from 5 to 90 km/h) on road segment i ; L_i is the length of road segment i (km); $EF_{v,s}$ is the emission

factor for type-v vehicles by vehicle speed s (Gg CO_2 km^{-1} per vehicle). The census identification numbers for road segments were used with Google Maps software to select point coordinates for each observed road segment, with the selected points being mapped to identify the same roads on the DRM. The information from the traffic census, such as road classification, daily traffic volume, and mean speed, were combined for the DRM road segments. The average traffic conditions for each road classification in each municipality unit [65] were substituted for the road segments not covered by the census. The L_i values were calculated from the DRM using a geographic information system (GIS) tool. The $EF_{v,s}$ values were obtained from Dohi et al. [66] (Table 3). Emissions were mapped on the center line of each road segment.

Area-source emissions

Area-source emissions included those from the industrial, commercial, residential, and agricultural sectors. The main source of industrial, commercial, and residential emissions is fuel consumption in buildings, for which the Hestia project [23] estimated non-electrical energy using the eQUEST simulation tool [67] by incorporating the building classification and age, with the building emissions based on the building total floor areas (TFAs) [68]. Since spatial data (building polygons) are not available for buildings of all ages in Japan, census data were used to allocate the emissions using building polygons (Fig. 2C) based on the TFAs.

Emissions from the industrial and commercial sector included those from fossil-fuel consumption by workers. Emissions from all areas in Tokyo, based on the economic census ($n = 5{,}318$), were calculated as follows:

$$E_{ic} = \sum_{i=1}^{n} \sum_{q} W_{q,i} \cdot \frac{TE_q}{TW_q}, \quad (7)$$

where E_{ic} represents the 2014 total emissions from the industrial and commercial sector (Gg CO_2); $W_{q,i}$ is the number of workers for category q in census area i (Table 4); TE_q is the total annual emissions for category q (Gg CO_2); and TW_q is the total number of workers in category q. The $W_{q,i}$ values for all of the categories in census areas were obtained from the 2014 economic census [69]. The census area comprised politically based blocks with an average area of around 0.5 km^2. The TW_q values were obtained from economic census data [69], and the TE_q values were extracted from the Tokyo energy-balance table [70]. The annual CO_2 emission factors by workers ($\frac{TE_q}{TW_q}$; Gg CO_2 per worker) were derived for each category (Table 4). The annual emissions from the fuels used in energy conversion (e.g., electricity generation and waste incineration) were not included in the energy-balance table [70] to avoid counting them twice. The reported total emissions for the industrial and commercial sector were used to derive emission factors and to calculate the emissions for each census area, similar to the approach used by Gately and Hutyra (2017) [19] for commercial emissions.

Total emissions were allocated to individual buildings in each census area, with all of the building polygons being associated to a given building use (industrial and commercial, or residential), using land-use maps covering four areas (23 wards in Tokyo, the Tama city area, Tama rural area, and island areas) at spatial resolutions of 3 × 3 m to 43 × 43 m [71]. The data on individual building polygons (e.g., site area (m^2), height (m), number of floors, and

floor area (m^2)) were obtained as follows. Each building site area was estimated from the building polygon maps, and the building height was estimated from the difference in heights between a raster-type digital surface model (DSM) [72] and a vector-type digital-elevation model (DEM) [73]. DSM v. 1.1 was based on digital photos from the Advanced Land Observing Satellite, with an accuracy within 5 m [72]. A 30 × 30 m DSM dataset was used with a 5 × 5 m DEM dataset (updated in 2016) based on airborne laser observations (2015), with an elevation accuracy within 0.7 m (standard deviation) [73]. The number of floors was estimated by dividing the building height by the average ceiling height (2.9 m for residential buildings, and 3.5 m for industrial and commercial buildings). The TFAs were estimated by multiplying the site area by the number of floors. The emission factors of the buildings (Gg CO_2 m^{-2}) in each census area were calculated by dividing the total emissions by the TFAs, aggregated over the census areas. Finally, the emissions from each industrial and commercial building were estimated by multiplying the emission factors by the TFAs of the individual buildings. Industrial and commercial emissions were mapped at the level of individual buildings.

Emissions from the residential sector were calculated for all of the population census areas in Tokyo ($n = 5{,}578$) by formula:

$$E_{re} = \sum_{i=1}^{n} \sum_{f,h,b} A_{h,b,i} \cdot EF_{f,h,b}, \quad (8)$$

where E_{re} represents the 2014 total emissions from the residential sector (Gg CO_2); $A_{h,b,i}$ is the number of households with occupancy h (with four categories: 1, 2, 3, or ≥4 occupants) in type b buildings (collective or detached) in the census area i; and $EF_{f,h,b}$ is the total annual emission intensity (Gg CO_2 yr^{-1} per household) of fuel type f, in household with occupancy h, and for building type b. The $A_{b,h,i}$ values were obtained from the 2015 population census data [74], and the $EF_{f,h,b}$ were from an investigation report on energy consumption in households as provided in Table 5 [75]. Finally, the total emissions from each census area were allocated to each building in proportion to the TFAs and with consideration of whether the buildings were collective or detached, and mapped at the level of individual buildings.

Agricultural emissions in this study are defined as emissions from fossil fuel use in agricultural machinery. The emissions processes were considered as those arising during crop planting, and those associated emissions were calculated for 62 municipalities in Tokyo as follows:

$$E_{am} = \sum_{i=1}^{n} \sum_{p} A_{p,i} \cdot EF_p, \quad (9)$$

where E_{am} represents the 2014 total emissions from agricultural machinery use (Gg CO_2); $A_{p,i}$ is the area for crop type p cultivated in municipality i (ha); and EF_p is the annual emission factor for farmland by crop type (Gg CO_2 ha^{-1}). The $A_{p,i}$ value for each Tokyo municipality was obtained from the agricultural census [76] and an investigation report on agricultural products in Tokyo [77], and the EF_p values were from a 2003 report [78] and an academic paper [79] (Table 6). Farmland was divided into two categories, rice paddy fields and other farmland, using a land-use map at a 10 × 10 m spatial resolution based on remote-sensing data for the 2006–2011 period [80]. Finally, the agricultural emissions mapped in each municipality [65] were sorted into a 10 × 10 m mesh for mapping based on the two types of farmland.

Data integration

Emission calculations and spatial emissions mapping/modeling were integrated using ArcGIS v. 10.4. The world geodetic system (1984) was used for mapping all of the emission sources, and a symbol tool was used here for visualizing the emissions on maps. A 3D map of the emission sources in SG Ward is shown in Fig. 2D as an example, allowing visualization of the emissions from local facilities, road segments, and buildings.

All of the data used, their versions or editions, and sources are summarized in Table S4. More than two million building polygons were used to produce emission maps around 500 MB in size. The emission maps were not gridded products since a multi-resolution approach was adopted. The original maps were converted to a 1 km mesh size (Fig. 3) for convenience in data handling.

Results and discussion

Total emissions from the Tokyo Metropolis

Tokyo is one of 47 prefectures in Japan and comprises 23 central city wards and multiple cities, towns, and villages (Table S2). The three highest point-source gridded emissions in 2014 occurred in SG, OT, and MN Wards at 6,183, 907, and 253 Gg CO_2 km^{-2}, respectively (Fig. 3A), due to two large power plants and a major airport being located within these areas. The highest line-source emissions occurred in KT, OT, and EG Wards at 155, 146, and 144 Gg CO_2 km^{-2}, respectively (Fig. 3B). The highest gridded emissions for area sources (Fig. 3C) occurred in CD, CO, and SJ Wards at 173, 168, and 164 Gg CO_2 km^{-2}, respectively. These high emissions are primarily due to the high floor numbers and large building areas for residential, industrial, and commercial use concentrated in these areas. A total emissions map is given in Fig. 3D, with the three highest emissions being 6,210 in SG Ward, 1,058 in OT Ward, and 295 Gg CO_2 km^{-2} in MN Ward, respectively.

The estimated total 2014 $FFCO_2$ emissions from Tokyo were 43,916 Gg CO_2 (Table 7), which comprised individual sector contributions of 16,323 from road transportation; 13,085 from the industrial and commercial sector; 6,478 from electricity generation; 5,302 from the residential sector; 1,483 from waste incineration; 940 from civil aviation; 279 from waterborne navigation; and 26 Gg CO_2 from the agricultural machine use sector. Total annual emissions from the area, line, and point sources were 18,413, 16,323, and 9,180 Gg CO_2, respectively.

The highest point-source emissions (Fig. 4) for 2014 were as follows. Power plants: Shinagawa (3,219), Oi (2,965), and Roppongi energy service (140 Gg CO_2) plants; Civil aviation: Haneda (907), Chofu (15), and Oshima (4 Gg CO_2) airports; Waterborne navigation: Tokyo (253), Mikurajima (5), and Okada (4 Gg CO_2) ports; and waste incineration plants: Tokyo Waterfront Recycle Power (188), Koto new plant (140), and Minato plant (89 Gg CO_2). The data for all 106 point sources are given in Table S1. The 19 power plants contributed 70.6% of the 2014 total point-source emissions (6,478), the 61 waste incineration plants 16.2% (1,483), the 11 airports 10.2% (940), and the 15 ports 3.0 % (279 Gg CO_2).

The highest line-source emissions for 2014 (Fig. 5) were associated with 30 road segments on two urban highways: Central loop line highway in KS Ward (19.7) and the Coastline highway in KT Ward (18.8 Gg CO_2 km^{-1}). The 2014 emissions from high-speed national

346 highways (total length 150 km) were 1,048 Gg CO_2 (6.4% of the total line-source emissions);
347 urban highways (576 km) 4,867 Gg CO_2 (29.8%); general national highways (726 km) 3,520
348 Gg CO_2 (21.6%); major regional roads (1,625 km) 4,761 Gg CO_2 (29.2%); and general
349 regional roads (1,614 km) 2,128 Gg CO_2 (13.0%).
350 The highest area-source emissions from the industrial and commercial sector for 2014 were
351 recorded in the inner-city areas in CD (172.4), CO (167.0), and SJ (162.0 Gg CO_2 km^{-2})
352 Wards (Fig. 6A), respectively. The industrial and commercial emissions counted from
353 economic census areas were shown in Fig. 6B. Those from the residential sector were in KT
354 (10.0), TS (9.9), and TT (9.5 Gg CO_2 km^{-2}) Wards (Fig. 7A), respectively. The residential
355 emissions counted from population census areas were shown in Fig. 7B. Those from the
356 agricultural sector (Fig. 8A) were recorded in MS (0.45) and NK Cities (0.36), and EG Ward
357 (0.33 Gg CO_2 km^{-2}), respectively. The agricultural emissions counted for 62 municipalities
358 (Fig. 8B) were finally allocated for high-spatial-resolution map (Fig. 8C).
359
360 **Comparison with other emission estimates made by different approaches**
361 The Tokyo government has reported annual GHG emissions every year since 1990, with
362 emissions being calculated with a top-down approach based on energy consumption [81]. In
363 the governmental EI, emissions for each sector in Tokyo are based on the final energy
364 consumption, including electricity, city gas, liquefied petroleum gas, and kerosene, with
365 emissions being apportioned according to economic indicators, such as family expenditure,
366 commodity values, numbers of vehicles, buildings areas, and passenger and cargo transport in
367 Tokyo.
368 Annual emissions between the present EI and the EI prepared by the Tokyo government are
369 compared for four major categories (Fig. 9A1-2). The governmental EI includes total
370 emissions from the Tokyo Metropolis of 62,120 Gg CO_2 for 2014. The governmental EI
371 includes the following emissions: 29,320 from the industrial and commercial sector; 19,650
372 from the residential sector; 11,570 from transportation; and 1,570 Gg CO_2 from waste
373 incineration. Based on the annual emissions by sector and fuel type in the report [81], we
374 derived the non-electric emissions for the residential sector from the governmental EI as
375 5,532, consistent with our result of 5,302 Gg CO_2. However, those for the industrial and
376 commercial sector are different (governmental EI 6,080, the present EI 13,085 Gg CO_2). For
377 waste incineration, the governmental EI considered only emissions from the fossil-carbon
378 content of waste (1,570), whereas we included both these emissions (1,473) and the
379 combustion agent (10 Gg CO_2).
380 The differences in emissions between the two EIs could be associated mainly with electricity
381 production. This study estimated the emissions from electricity generation as point sources
382 based on fossil-fuel consumption at power plants (direct emissions, Scope-1[6]), while the
383 Tokyo government estimated them based on the final energy consumption (consumption-
384 based emissions, Scope-2 [6]). For example, the government EI includes emissions from
385 electricity consumption by railways and the electricity generated outside the Tokyo area [82].
386 These differences resulted in higher annual emissions from electricity consumption in the
387 government EI (39,460) compared with the EI of the present study (6,478 Gg CO_2).
388 The EAGrid is a reliable EI for multiple pollutants that was developed for the East Asia
389 region in 1995 [83] and revised in 2000 with a focus on local emission sources in Japan

(EAGrid-Japan 2000) [84]. In the most recent version (2010), emissions were estimated by adjusting the 2000 emissions according to the increase in national fuel consumption from 2000 to 2010 (see Fukui et al. [85]), without any change in the distribution of emission sources. Here we relied on data for the Tokyo domain provided by the developer of EAGrid-Japan 2010 [85].

Total emissions in the EAGrid-Japan 2010 EI for Tokyo are 42,009, which is 4.3% lower than our estimate for 2014 (43,916 Gg CO_2). The Tokyo Statistical Yearbook 2015 [86] records increases in population and gross regional product in Tokyo during 2010–2014 of 1.7% and 3.9%, respectively. The difference between the two EIs may be related to the change in population and economic growth over the four year period. To compare the two sets of results by source type, the sectoral emissions of the present EI in three categories are summarized in Fig. 9B1 and those for EAGrid are shown in Fig. 9B2. The point-source emissions of EAGrid (5,631 Gg CO_2) include those from power plants, waste incineration plants, vessels, and aircraft; line sources from road transportation (14,672 Gg CO_2); and area sources (21,705 Gg CO_2) from residential and commercial combustion equipment, factory and building boilers, off-road transportation (construction, agricultural, and factory machine use), open burning, and facilities.

Spatial distributions of the emissions between the two EIs were compared at a 1 × 1 km resolution by scaling the total EAGrid emissions to our 2014 EI (Fig. 10). The difference in the point sources (Fig. 10A) shows that some gridded emissions of this study were lower than those in EAGrid. To map the gridded values of EAGrid, the counted total emissions from each airport and port were allocated according to the number of persons engaged in the related industry groups (Table S5), with the number of point sources being higher than those in this study. Other differences are due to the EAGrid EI, which does not include recently constructed major sources, such as Shinagawa power plant and Haneda airport domestic terminal 2. As shown in Fig. 11A, the correlation of the gridded emissions of point sources between the two sets of results is very low ($R^2 = 0.42$).

Line-source differences (Fig. 10B) vary from –100 to +100 Gg CO_2 km^{-2}. Differences in emission factors for vehicles and the counting approach for the total travel distance caused the difference in emission estimates. The number of vehicles from the traffic census 2000 and the average travel distance per vehicle were used to estimate the travel distance in EAGrid-Japan 2000 [84], whereas our assessment was based on the road length from the 2015 DRM and the traffic volume from the traffic census 2015. Area-source differences (Fig. 10C) are variable because the EAGrid EI includes residential, industrial, commercial, off-road, open burning, and other emissions as area sources, whereas this study only considers residential, industrial and commercial, and agricultural sectors as area sources. The area-source emissions in the present EI were 3,292 Gg CO_2, lower than those of the EAGrid. As shown in Fig. 11B-C, the correlations of the gridded emissions for line and area sources between the two sets of results are high ($R^2 = 0.74$ for line sources and 0.71 for area sources).

Differences in total emissions vary between –700 and +4,500 Gg CO_2 km^{-2} (Fig. 10D), with differences being smaller in the western mountain and forest areas and larger in the inner-city areas (eastern Tokyo). As shown in Fig. 11D, the correlation of the total gridded emissions between the two sets of results is moderate ($R^2 = 0.69$). The number of cells in the present EI is much greater than that in EAGrid in the 0–10 Gg CO_2 km^{-2} emission range (Fig. 12), with

the present EI therefore including more low-emission areas than the EAGrid, while greater 10–50 Gg CO_2 km^{-2} emissions are included in the latter. The numbers of cells are consistent for the other emission ranges. Thus, we could conclude that even the number of cells in some emission ranges and the total annual emissions between the two sets of results seem to be close but the distributions of the source emissions are different.

The Open-source Data Inventory for Anthropogenic CO_2 (ODIAC) [18] provides emissions with less detailed patterns from inner-city areas (eastern Tokyo) to the western mountains and forested areas in Tokyo in 2014 (Fig. 13A). Such characteristic emission distributions are also reported in other urban areas [15, 25, 88]. Differences in gridded annual emissions between our study and ODIAC ranged from about –800 to +3,300 Gg CO_2 $cell^{-1}$ (Fig. 13B), with differences being greater in inner-city areas. The blue-color grids (Fig. 13B) indicate the three most negative values in densely populated areas. The ODIAC 2014 estimated higher total emissions over these areas, while our estimates were lower. The red-color grids (Fig. 13B) indicate the three highest positive values, where two power plants (the Shinagawa and Oi plants, with 3,219 and 2,965 Gg CO_2, respectively) and an international airport (Tokyo Haneda Airport, with 940 Gg CO_2) are located (Table S1). It is clear that ODIAC 2014 does not include such large point sources. We emphasize that local activity data are critical in capturing spatial patterns of local emissions in urban areas.

Current limitations and future perspectives

Uncertainties associated with emission factors, activity data, and emission spatial modeling introduce uncertainties in the final emission estimates [e.g., 24, 89]. We refer to the uncertainties on the basis of activity data and emission factors (Table S6) using IPCC guidelines [33, 90]. The total uncertainty is estimated to be ±3.57%, equivalent to 43,916 ± 1,568 Gg CO_2.

Uncertainties introduced from emissions calculations and mapping processes are likely to be large due to the assumptions and approximations used. For example, the operation ratio of power plants varies with individual plants; however, this study applied averaged utilization efficiency for the whole plants in the calculation process. This approach reduces the variability in emissions at each power plant, leading to poor representation of emissions with higher temporospatial resolution than we applied here. The road segments that are not fully covered by the census contribute over 4,205 km in our calculation. We substituted the average traffic conditions for the road segments to estimate the emissions. This approach could overestimate the traffic quantities and emissions for the segments.

In mapping processes, this study treated the mobile emissions of aircraft and vessels as point sources. This means that the whole emissions over their moving paths were aggregated to a point, leading to an overestimate of the point-source emissions. The building emissions were estimated using TFAs of buildings in each census area. In this estimate we used DSM data with a spatial resolution of 30 m, but this spatial resolution is insufficient to calculate the heights and TFAs for individual buildings. Additionally, our downscale approach did not distinguish occupied and vacant houses. All of these limitations should be improved in the next study. As in previous studies (e.g., Hestia [23]), better data availability for emissions calculations and mapping should greatly improve the accuracy of estimates.

We plan to update our emission estimates once updated activity data become available. The methods employed here are applicable to other parts of Japan, and the entire country could be covered, although further objective evaluation is necessary. Future work should also include improvements of the methodology for mapping emissions from traffic on narrow roads, modeling of temporal variations (seasonal, weekly, and diurnal), and extending the time period of this study.

Conclusions

Spatially explicit estimates of $FFCO_2$ emissions were prepared for the Tokyo Metropolis, with the EI being primarily compiled using a bottom-up approach. Following the 2006 IPCC guidelines, geolocation data were collected for point, line, and area sources, with the emissions mapped where possible. Detailed activity data, including the utilization efficiency of power plants, load factors of vessels, fossil-carbon contents of waste, and emission factors for fossil-fueled power generation, aircraft movements, navigation, and combustion processes, were utilized to improve the accuracy of emission estimates. The utilization of spatially verified national census data, regional/city specific emission factors, and emission factors for road segments, as well as the consideration of low-emission sectors, such as waterborne navigation and agricultural machinery use, were highlighted. This EI demonstrated that the Tier 3 approach could be applicable not only at a national scale but also a sub-national scale.

The total emissions from the Tokyo Metropolis in 2014 were estimated to be 43,916 Gg CO_2. The highest emission sector was road transportation (16,323 Gg CO_2), which accounted for 37.2% of the total emissions. Spatial emission patterns were compared with those of EAGrid-Japan and ODIAC, highlighting differences in the distributions of source types. The differences resulted mainly from the counting and mapping approaches used, and the different sector categories.

This methodology is applicable to other prefectures and can be used to cover the entire country. This EI facilitates the acquisition of information on emissions from high-emission point sources, buildings, and road segments more than other gridded datasets. It may also be used to validate other EIs and to prepare urban carbon budgets in addition to aiding policy makers in controlling GHG emissions.

Abbreviations

CO_2: carbon dioxide

$FFCO_2$: carbon dioxide emissions from fossil fuel combustion

EI: emission inventory

GPC: Global Protocol for Community-Scale Greenhouse Gas Emission Inventories

UNFCCC: UN Framework Convention on Climate Change

IPCC: Intergovernmental Panel on Climate Change

GHG: greenhouse gas

PB: purely geographic-based

EAGrid-Japan: East Asian Air Pollutant Emission Grid Database for Japan

ODIAC: Open-source Data Inventory for Anthropogenic CO_2

MW: megawatt

LTO: landing and take-off

ICAO: International Civil Aviation Organization

GT: gross tonnage

MSW: municipal solid waste

CA: combustion agent

DRM: digital road map

GIS: geographic information system

TFA: total floor area

DSM: digital surface model

DEM: digital elevation model

Declarations

Ethics approval and consent to participate

Not applicable.

Consent for publication

Not applicable.

Availability of data and materials

The data used in this study are either presented in this manuscript or available from the data source indicated. The authors plan to make the data product developed in this study publicly available with a DOI.

Competing interests

The authors declare that they have no competing interests.

Funding

This study was funded by the Ministry of the Environment, Japan, and partly supported by the Low-Carbon Research Program of the National Institute for Environmental Studies.

Authors' contributions

RC carried out the data collection and analysis with support from MS. TF provided the EAGrid-Japan2010 emission inventory and guidance on the use of the inventory in the data analysis. RC wrote the manuscript with input from MS. RC and AI provided critical comments that shaped the study and manuscript. All the authors contributed to the final version of the manuscript and approved the submission.

Acknowledgements

We thank Tomohiro Oda who conceived this study, and provided valuable input and feedback to the data analysis and manuscript development. The authors also acknowledge that this study greatly benefited from the Master's thesis work conducted by Yutaka Mori at Osaka University under the supervision of Tomohiro Oda. We thank Shamil Maksyutov from the National Institute for Environmental Studies for his valuable comments on this article. The high-resolution land use data used for this paper have been provided by HRLULC of the Japan Aerospace Exploration Agency.

Authors' information

Affiliations

Center for Global Environmental Research, National Institute for Environmental Studies, 16-2, Onogawa, Tsukuba, Ibaraki, 305-8506, Japan

Richao Cong, Makoto Saito, Ryuichi Hirata & Akihiko Ito

Fukushima Branch, National Institute for Environmental Studies, Fukushima Environmental Creation Centre, 10-2, Fukasaku, Miharu Town, Tamura District, Fukushima, 963-7700, Japan

Richao Cong

Institute of Behavioral Sciences, 2-9, Ichigaya-honmuracho, Shinjuku-ku, Tokyo, 162-0845, Japan

Tetsuo Fukui

Corresponding authors

Correspondence to Richao Cong or Makoto Saito.

References

1. Le Quéré C, Andrew RM, Friedlingstein P, Sitch S, Pongratz J, Manning AC, et al. Global Carbon Budget 2017. Earth Syst Sci Data. 2018;10:405-48. https://doi.org/10.5194/essd-10-2141-2018.
2. UN-Habitat. The challenge. https://unhabitat.org/topic/climate-change. Accessed 1 Jan 2020.
3. Hoornweg D, Sugar L, Gómez CLT. Cities and greenhouse gas emissions: moving forward. Environ Urban. 2011;23:207–27.
4. C40 Cities Climate Leadership Group. https://www.c40.org/. Accessed 1 Jan 2020.
5. Global Covenant of Mayors for Climate & Energy. https://www.globalcovenantofmayors.org/. Accessed 1 Jan 2020.
6. Fong WK, Sotos M, Michael Doust M, Schultz S, Marques A, Deng-Beck C, et al. Global Protocol for Community-Scale Greenhouse Gas Emission Inventories. 2015. http://ghgprotocol.org/greenhouse-gas-protocol-accounting-reporting-standard-cities. Accessed 1 Jan 2020.
7. United Nations. Paris Agreement. 2015. https://unfccc.int/process-and-meetings/the-paris-agreement/what-is-the-paris-agreement. Accessed 1 Jan 2020.
8. United Nations. Kyoto Protocol to the United Nations Framework Convention on Climate Change. 1998. https://unfccc.int/process-and-meetings/the-kyoto-protocol/what-is-the-kyoto-protocol/what-is-the-kyoto-protocol. Accessed 1 Jan 2020.
9. Xi F, Geng Y, Chen X, Zhang Y, Wang X, Xue B, et al. Contributing to local policy making on GHG emission reduction through inventorying and attribution: A case study of Shenyang, China. Energy Policy. 2011. https://doi.org/10.1016/j.enpol.2011.06.063.
10. Markolf SA, Matthews HS, Azevedo IL, Hendrickson C. An integrated approach for estimating greenhouse gas emissions from 100 US metropolitan areas. Environ Res Lett. 2017;12(2):024003.
11. Minx J, Baiocchi G, Wiedmann T, Barrett J, Creutzig F, Feng K, et al. Carbon footprints of cities and other human settlements in the UK. Environ Res Lett. 2013;8(3):035039.

12. Wiedmann TO, Chen G, Barrett J. The concept of city carbon maps: a case study of Melbourne, Australia. J Ind Ecol. 2016;20(4):676-91.
13. Chavez A, Ramaswami A. Articulating a trans-boundary infrastructure supply chain greenhouse gas emission footprint for cities: Mathematical relationships and policy relevance. Energy Policy. 2013;54:376.
14. Qi C, Wang Q, Ma X, Ye L, Yang D, Hong J. Inventory, environmental impact, and economic burden of GHG emission at the city level: case study of Jinan, China. J Clean Prod. 2018;192:236-43.
15. Gurney KR, Liang J, O'Keeffe D, Patarasuk R, Hutchins M, Huang J, et al. Comparison of Global Downscaled Versus Bottom-Up Fossil Fuel CO_2 Emissions at the Urban Scale in Four US Urban Areas. J Geophys Res Atmos. 2019. https://doi.org/10.1029/2018JD028859.
16. Boden TA, Marland G, Andres RJ. Global, Regional, and National Fossil-Fuel CO2 Emissions (Vol. 53, pp. 1689–1699). Oak Ridge, TN: Carbon Dioxide Information Analysis Center, Oak Ridge National Laboratory, U.S. Department of Energy. 2017. https://doi.org/10.3334/CDIAC/00001_V2017. Accessed 1 Jan 2020.
17. Crippa M, Solazzo E, Huang G, Guizzardi D, Koffi E, Muntean M, et al. High resolution temporal profiles in the Emissions Database for Global Atmospheric Research. Sci Data. 2020. https://doi.org/10.1038/s41597-020-0462-2.
18. Oda T, Maksyutov S, and Andres RJ. The Open-source Data Inventory for Anthropogenic CO_2, version 2016 (ODIAC2016): a global monthly fossil fuel CO_2 gridded emissions data product for tracer transport simulations and surface flux inversions. Earth System Science Data. 2018. https://doi.org/10.5194/essd-10-87-2018.
19. Gately CK, Hutyra LR. Large Uncertainties in Urban-Scale Carbon Emissions. J Geophys Res Atmos. 2017;122:242-60.
20. Gurney KR, Razlivanov I, Song Y, Zhou Y, Benes B, Abdul-Massih M. Quantification of fossil fuel CO_2 emissions on the building/street scale for a large US city. Environ Sci Technol. 2012. http://doi.org/10.1021/es3011282.
21. Gurney KR, Patarasuk P, Liang J, Song Y, O'Keeffe D, Rao P, et al. The Hestia fossil fuel CO_2 emissions data product for the Los Angeles megacity (Hestia-LA), Earth Syst. Sci. Data. 2019. https://doi.org/10.5194/essd-11-1309-2019.
22. Patarasuk P, Gurney KR, O'Keeffe D, Song Y, Huang J, Rao P, et al. Urban high-resolution fossil fuel CO_2 emissions quantification and exploration of emission drivers for potential policy applications. Urban Ecosyst. 2016. https://doi.org/10.1007/s11252-016-0553-1.
23. The Hestia Project. http://hestia.project.asu.edu/audience_researchers.shtml. Accessed 1 Jan 2020.
24. Bun R, Nahorski Z, Horabik-Pyzel J, Danylo O, See L, Charkovska N, et al. Development of a high-resolution spatial inventory of greenhouse gas emissions for Poland from stationary and mobile sources. Mitig Adapt Strateg Glob Chang. 2018. https://doi.org/10.1007/s11027-018-9791-2.

25. Oda T, Bun R, Kinakh V, Topylko P, Halushchak M, Marland G, et al. Errors and uncertainties in a gridded carbon dioxide emissions inventory. Mitig Adapt Strateg Glob Chang. 2019;24(6):1007-50.
26. Topylko P, Lesiv R, Bun R, Zahorski Z, Horabik J. Geoinformation technology for spatial inventory of greenhouse gas emissions: electricity and heat generation in Poland. Econtechmod. 2013;2:51-58.
27. Charkovska N, Halushchak M, Bun R, Nahorski Z, Oda T, Jonas M, et al. A high-definition spatially explicit modelling approach for national greenhouse gas emissions from industrial processes: reducing the errors and uncertainties in global emission modelling. Mitig Adapt Strateg Glob Change. 2019;24:907-39.
28. Danylo O, Bun R, See L, Charkovska N. High-resolution spatial distribution of greenhouse gas emissions in the residential sector. Mitig Adapt Strateg Glob Chang. 2019;24(6):941-67.
29. Rao P, Gurney KR, Patarasuk R, Song Y, Miller CE, Duren RM, et al. Spatio-temporal Variations in on-road CO_2 Emissions in the Los Angeles Megacity. AIMS Geosciences. 2017;3(2):239-67. https://doi.org/10.3934/geosci.2017.2.239.
30. Gately CK, Hutyra LR, Wing IS. Cities, traffic, and CO_2: A multidecadal assessment of trends, drivers, and scaling relationships. Proc. Natl. Acad. Sci. U. S. A. 2015;112(16):4999-5004.
31. Boychuk P, Nahorski Z, Boychuk K, Horabik J. Spatial analysis of greenhouse gas emissions in road transport of Poland. Econtechmod. 2012;1(4):9-15.
32. Mori Y. Development of high spatial- and temporal- resolution anthropogenic CO_2 inventory in Osaka Prefecture (Master thesis). 2016. http://www.see.eng.osaka-u.ac.jp/seege/seege/material/2016/mori.pdf. Accessed 1 Jan 2020.
33. IPCC. 2006 IPCC Guidelines for National Greenhouse Gas Inventories. 2007. https://www.ipcc-nggip.iges.or.jp/public/2006gl/. Accessed 1 Jan 2020.
34. Electrical Japan. Fossil fuel fired power generation information. 2017. http://agora.ex.nii.ac.jp/earthquake/201103-eastjapan/energy/electrical-japan/area/13.html.ja. Accessed 1 Jan 2020. **(in Japanese)**
35. Tokyo Gas Engineering Solutions. The list of plants built under the redevelopment. http://www.tokyogas-es.co.jp/case/#anchor08. Accessed 1 Jan 2020. **(in Japanese)**
36. Tokyo electric power company holdings. The list of power plants: steam and internal combustion types. http://www.tepco.co.jp/corporateinfo/illustrated/electricity-supply/index-j.html. Accessed 1 Jan 2020. **(in Japanese)**
37. Mori building. The introduction for Roppongi energy service plant. https://www.mori.co.jp/morinow/2011/05/20110512160000002184.html. Accessed 1 Jan 2020. **(in Japanese)**
38. Agency for Natural Resources and Energy. Running ratio of fossil-fueled power plants in 2014. 2015. https://www.enecho.meti.go.jp/statistics/electric_power/ep002/xls/2014/2-4-H26.xls. Accessed 1 Jan 2020. **(in Japanese)**
39. Agency for Natural Resources and Energy. Energy consumption and electricity generation amount by power plants. 2014. https://www.enecho.meti.go.jp/statistics/electric_power/ep002/xls/2014/4-1-H26.xls. https://www.enecho.meti.go.jp/statistics/electric_power/ep002/xls/2014/4-2-H26.xls.

https://www.enecho.meti.go.jp/statistics/electric_power/ep002/xls/2014/4-3-H26.xls. Accessed 1 Jan 2020. **(in Japanese)**

40. Ministry of the Environment. Guidelines for Calculation Method on Greenhouse Gas Emissions. 2017. https://ghg-santeikohyo.env.go.jp/files/manual/chpt2_4-4.pdf. Accessed 1 Jan 2020. **(in Japanese)**
41. Ministry of Land, Infrastructure, Transport and Tourism. Annual record of airport management. 2015. http://www.mlit.go.jp/common/001296737.xls. Accessed 1 Jan 2020. **(in Japanese)**
42. Toho Air Service. Safety report for 2015: the types of helicopters. http://www.tohoair.co.jp/english/index.html. Accessed 1 Jan 2020. **(in Japanese)**
43. New Central Airservice. Safety report for 2015: the types of aircrafts. https://www.central-air.co.jp/en/index.html. Accessed 1 Jan 2020. **(in Japanese)**
44. Air Do. Safety report for 2015. https://www.airdo.jp/en/. Accessed 1 Jan 2020. **(in Japanese)**
45. All Nippon Airways. ANA group safety report for 2015. https://www.ana.co.jp/en/jp/. Accessed 1 Jan 2020. **(in Japanese)**
46. Japan Airlines. JAL safety report for 2015. http://www.jal.com/en/. Accessed 1 Jan 2020. **(in Japanese)**
47. Skymark Airlines. Safety report for 2015. https://www.skymark.jp/en/. Accessed 1 Jan 2020. **(in Japanese)**
48. Solaseed Air. Safety report for 2015. https://www.solaseedair.jp/en/. Accessed 1 Jan 2020. **(in Japanese)**
49. Starflyer. Safety report for 2015. https://www.starflyer.jp/en/. Accessed 1 Jan 2020. **(in Japanese)**
50. Flugzeuginfo.net. Aircraft types. 2017. http://www.flugzeuginfo.net/acdata_en.php. Accessed 1 Jan 2020.
51. Haneda Airport International Passenger Terminal. Domestic flight information. 2017. http://www.tokyo-airport-bldg.co.jp/en/flight/. Accessed 1 Jan 2020.
52. Haneda Airport International Passenger Terminal. International flight information. 2017. http://www.haneda-airport.jp/inter/flight/showFlightScheduleSearch?langId=en. Accessed 1 Jan 2020.
53. European Union Aviation Safety Agency. ICAO Aircraft Engine Emissions Databank. 2017. https://www.easa.europa.eu/sites/default/files/dfu/edb-emissions-databank%20v26B-NewFormat%20%28web%29.xlsx. Accessed 1 Jan 2020.
54. Federal Office of Civil Aviation. Guidance on the Determination of Helicopter Emissions. 2013. https://www.bazl.admin.ch/dam/bazl/de/dokumente/Fachleute/Regulationen_und_Grundlagen/guidance_on_the_determinationofhelicopteremissions.pdf.download.pdf/guidance_on_the_determinationofhelicopteremissions.pdf. Accessed 1 Jan 2020.
55. Ministry of the Environment. The emissions from ships. 2011. https://www.env.go.jp/chemi/prtr/result/todokedegaiH28/syosai/14.pdf. Accessed 1 Jan 2020. **(in Japanese)**
56. OPRI. Investigation report on the environmental impact of PM by vessels. 2007. http://fields.canpan.info/report/download?id=3269. Accessed 1 Jan 2020. **(in Japanese)**

57. Ministry of Land, Infrastructure, Transport and Tourism. Annual report on vessels at Tokyo port. https://www.mlit.go.jp/common/001277697.xls. Accessed 1 Jan 2020. **(in Japanese)**
58. Bureau of Port and Harbor. Annual report on vessels on ports from the islands. https://www.kouwan.metro.tokyo.lg.jp/yakuwari/27kousei_7_2.xls. Accessed 1 Jan 2020. **(in Japanese)**
59. Clean Authority of Tokyo. Waste disposal of Tokyo 23cities: Annual report on the waste incineration plants of Tokyo in 2014. 2016. https://www.union.tokyo23-seisou.lg.jp/gijutsu/gijutsu/kumiai/shiryo/documents/26honbun.pdf. Accessed 1 Jan 2020. **(in Japanese)**
60. Ministry of the Environment. Investigation result on the municipal solid waste disposal status of Tokyo in 2014. 2017. http://www.env.go.jp/recycle/waste_tech/ippan/h26/data/seibi/city/13.xlsx. Accessed 1 Jan 2020. **(in Japanese)**
61. Bureau of Environment Tokyo Metropolitan Government. Investigation Report on the Status of Industrial Waste of Tokyo in 2014. 2016. https://www.kankyo.metro.tokyo.lg.jp/resource/industrial_waste/notification/investigation.files/H26houkokusyo.pdf. Accessed 1 Jan 2020. **(in Japanese)**
62. Bureau of Environment Tokyo Metropolitan Government. Waste disposal facilities in Tokyo. 2017. https://www.kankyo.metro.tokyo.lg.jp/resource/general_waste/processing_plant/processing_plant.files/20200101_shisetsulist.pdf. Accessed 1 Jan 2020. **(in Japanese)**
63. Ministry of Land, Infrastructure, Transport and Tourism. Traffic Census. 2015. http://www.mlit.go.jp/road/census/h27/data/xlsx/kasyo13.xlsx. Accessed 1 Jan 2020. **(in Japanese)**
64. Japan Digital Road Map Association. Digital road map. 2017. https://www.drm.jp/english/. Accessed 1 Jan 2020.
65. Ministry of Land, Infrastructure, Transport and Tourism. National Land Numerical Information Download Service: Administrative zones data. 2014. http://nlftp.mlit.go.jp/ksj-e/gml/datalist/KsjTmplt-N03-v2_3.html. Accessed 1 Jun 2019.
66. Dohi M, Shinri S, Masamichi T. Renewal of the Emission Factor of Carbon Dioxide and Fuel Consumption for Motor Vehicles. Technical note of NILIM. 2012;54:40-5. www.pwrc.or.jp/thesis_shouroku/thesis_pdf/1204-P040-045_dohi.pdf. Accessed 1 Jan 2020. **(in Japanese)**
67. United States Department of Energy. eQUEST. 2009. http://doe2.com/equest/index.html. Accessed 1 Jan 2020.
68. Zhou Y, Gurney K. A new methodology for quantifying on-site residential and commercial fossil fuel CO_2 emissions at the building spatial scale and hourly time scale. Carbon Manag. 2010;1:45-56.
69. Statistics Japan. 2014 Economic Census. 2016. http://www.stat.go.jp/english/data/e-census/index.html. Accessed 1 Jan 2020.
70. Agency for Natural Resources and Energy. Energy-balance table of Tokyo. 2017. https://www.enecho.meti.go.jp/statistics/energy_consumption/ec002/xls/13tokyo.xls. Accessed 1 Jan 2020. **(in Japanese)**

71. Bureau of Urban Development Tokyo Metropolitan Government. Land use of Tokyo. 2014. https://www.toshiseibi.metro.tokyo.lg.jp/seisaku/tochi_c/pdf/tochi_5/tochi_all.pdf. Accessed 1 Jan 2020. **(in Japanese)**
72. Japan Aerospace Exploration Agency. ALOS Global Digital Surface model (AW3D30). 2015. https://www.eorc.jaxa.jp/ALOS/en/aw3d30/data/index.htm. Accessed 1 Jan 2020.
73. Geospatial Information Authority of Japan, Building polygons and digital elevation model. 2017. https://fgd.gsi.go.jp/download/menu.php. Accessed 1 Jan 2020. **(in Japanese)**
74. Statistics Japan. 2015 Population Census. 2017. http://www.stat.go.jp/english/data/kokusei/index.html. Accessed 1 Jan 2020.
75. Statistics Japan. Investigation in 2014-2015 for counting the CO_2 emissions from households. 2016. https://www.e-stat.go.jp/en. Accessed 1 Jan 2020. **(in Japanese)**
76. Statistics of Tokyo. Investigation result on Agricultural census in Tokyo 2015. 2017. https://www.toukei.metro.tokyo.lg.jp/nourin/2015/ng15ta1400.xls. Accessed 1 Jan 2020. **(in Japanese)**
77. Tokyo Development Foundation for Agriculture, Forestry, and Fisheries. Investigation on the condition of agricultural products in Tokyo 2014. 2016. https://tokyogrown.jp/learning/library/img/agriculture_report_2014.pdf. Accessed 1 Jan 2020. **(in Japanese)**
78. National Institute for Agro-Environmental Sciences. Life Cycle Assessment for Environmentally Sustainable Agriculture. NIAES Report. 2003. http://www.naro.affrc.go.jp/archive/niaes/project/lca/lca_r.pdf. Accessed 1 Jun 2019. **(in Japanese)**
79. Shimizu N, Yuyama Y. Analysis of the energy consumption and profitability of agricultural practice with environmental consciousness-a case study in north-eastern Chiba Prefecture. J Rural Plan Assoc. 2007;26:365-70. https://www.jstage.jst.go.jp/article/arp/26/Special_Issue/26_Special_Issue_365/_article/-char/en. Accessed 1 Jan 2020. **(abstract in English and text in Japanese)**
80. Japan Aerospace Exploration Agency. Homepage of High-resolution Land Use and Land Cover Map Products: HRLULC 10m resolution map of Japan [2006-2011] (ver.16.09). 2016. http://www.eorc.jaxa.jp/ALOS/en/lulc/lulc_index.htm. Accessed 1 Jan 2020.
81. Bureau of Environment Tokyo Metropolitan Government. Final Energy Consumption and Greenhouse Gas Emissions in Tokyo (FY 2014). 2017. https://www.kankyo.metro.tokyo.lg.jp/en/climate/index.files/b0548c2a69e7883f1945aca50f606a92.pdf. Accessed 1 Jan 2020.
82. Agency for Natural Resources and Energy. Actual conditions on power generation and transmission. 2017. https://www.enecho.meti.go.jp/statistics/electric_power/ep002/xls/2014/2-5-H26.xls. Accessed 1 Jan 2020. **(in Japanese)**
83. Tonooka Y, Kannari A, Higashino H, Murano K. NMVOCs and CO emission inventory in East Asia. Water Air and Soil Pollut. 2001;130:199-204.
84. Kannari A, Tonooka Y, Baba T, Murano K. Development of multiple-species 1km× 1km resolution hourly basis emissions inventory for Japan. Atmos Environ. 2007. https://doi.org/10.1016/j.atmosenv.2006.12.015.

85. Fukui T, Kokuryo K, Baba T, Kannari A. Updating EAGrid2000-Japan emissions inventory based on the recent emission trends. J Jpn Soc Atmos Environ. 2014;49:117-25. https://www.jstage.jst.go.jp/article/taiki/49/2/49_117/_article. Accessed 1 Jan 2020. **(abstract in English and text in Japanese)**
86. Bureau of Environment Tokyo Metropolitan Government. Tokyo Statistical Yearbook 2015. 2017. https://www.toukei.metro.tokyo.lg.jp/tnenkan/tn-index.htm. Accessed 1 Jan 2020. **(in Japanese)**
87. Kannari A, Kokuryo K. Thirty-year histories of atmospheric emissions from road vehicles in Japan. J Jpn Soc Atmos Environ. 2013;48:20-34. https://doi.org/10.11298/taiki.48.20. Accessed 1 Jan 2020. **(abstract in English and text in Japanese)**
88. Chen J, Zhao F, Zeng N, Oda T. Comparing a global high-resolution downscaled fossil fuel CO_2 emission dataset to local inventory-based estimates over 14 global cities. Carbon Balance Manag. 2020. https://doi.org/10.1186/s13021-020-00146-3.
89. Hogue S, Marland E, Andres RJ, Marland G, Woodard D. Uncertainty in gridded CO_2 emissions estimates. Earth' Future. 2016. https://doi.org/10.1002/2015EF000343.
90. IPCC. Good Practice Guidance and Uncertainty Management in National Greenhouse Gas inventories. 2000. https://www.ipcc-nggip.iges.or.jp/public/gp/english/. Accessed 1 Jan 2020.

Figure captions

Fig. 1. Conceptual framework for emission mapping.

Fig. 2. Examples of vector maps for emission sources in SG Ward, Tokyo. (A) Locations of point emission sources. (B) Road segments for line sources. (C) Building polygons for area sources (blue line shows the boundary of the area). (D) 3D emission map for all sources (Gg CO_2 yr^{-1} per road segment for road emissions and Gg CO_2 yr^{-1} per polygon for others).

Fig. 3. Emission maps with 1 × 1 km mesh for (A) point sources, (B) line sources, (C) area sources, and (D) all sources. Unit: Gg CO_2 km^{-2} yr^{-1}.

Fig. 4. Map of 106 point sources in Tokyo (areas in blue frames indicate islands). The point in cyan indicates the highest emissions at Shinagawa power plant (3,219 Gg CO_2 yr^{-1}).

Fig. 5. Map of emissions from line sources for each road segment. The 30 road segments with the highest emissions are marked in black. Unit: Gg CO_2 km^{-1} yr^{-1}.

Fig. 6. Map of emissions from the industrial and commercial sector with (A) 1 × 1 km mesh, unit: Gg CO_2 km^{-2} yr^{-1}; (B) 5,318 economic census areas, unit: Gg CO_2 yr^{-1}. The municipality boundary for the area with the highest annual emissions (up to 82.2 Gg CO_2) is marked in cyan.

Fig. 7. Map of emissions from the residential sector with (A) 1 × 1 km mesh, unit: Gg CO_2 km^{-2} yr^{-1}; (B) 5,578 population census areas, unit: Gg CO_2 yr^{-1}. The municipality boundary for the area with the highest annual emissions (up to 6.6 Gg CO_2) is marked in cyan.

Fig. 8. Maps of emissions from the agricultural machine use sector with (A) 1 × 1 km mesh, unit: Mg CO_2 km^{-2} yr^{-1}. (B) 62 municipalities, unit: Mg CO_2 yr^{-1}. The area with the highest annual emissions (2,765 Mg CO_2 yr^{-1}) is marked in cyan. (C) high-spatial-resolution map on a grid with cell size of 10 × 10 m, unit: Kg CO_2 yr^{-1} per cell.

Fig. 9. Comparisons on annual CO_2 emissions in Tokyo between the present EI (A-1) and Tokyo government 2014 EI (A-2), and between the present EI (B-1) and EAGrid-Japan 2010 (B-2). Unit: Gg CO_2.
Note: In A-1, the industrial and commercial category includes emissions from the industrial and commercial sector and the electricity generation sector. The transportation category includes emissions from the road transportation, civil aviation, and waterborne navigation sectors.
In A-2, the transportation category includes emissions from the railway, road transportation, civil aviation, and waterborne navigation sectors.
In B-2, point sources include power plants, waste incineration plants, vessels, and aircrafts. Line sources refer to road transportation. Area sources include residential and commercial combustion equipment, factory and building boilers, off-road transportation, open burning, and facilities without identified locations.

Fig. 10. Differences in emissions between the present EI and 2010 EAGrid-Japan EI at a resolution of 1 × 1 km for: (A) point sources, (B) line sources, (C) area sources, and (D) all sources. Unit: Gg CO_2 km^{-2} yr^{-1}. (Difference = emissions from the present EI – 2010 EAGrid-Japan EI, after adjustment of EAGrid emissions, as described in the text.).

Fig. 11. Scatter plots of gridded emissions by source types between the present EI and EAGrid for: (A) point sources, (B) line sources, (C) area sources, and (D) all sources. Unit: $\log_{10}$ Gg CO_2 km^{-2} yr^{-1}.

Fig. 12. Frequency distribution of gridded emissions (Gg CO_2 km^{-2} yr^{-1}) for this study (green) and EAGrid-Japan 2010 adjusted (blue). n = 2,688.

Fig. 13. Emission maps with a 30 × 30 arcsec mesh size for (A) ODIAC 2014 clipped for the Tokyo domain, (B) gridded emission differences between this study and ODIAC 2014 clipped for the Tokyo domain (Difference = emissions from the present EI minus ODIAC 2014). Unit: Gg CO_2 yr^{-1} $cell^{-1}$.

Table captions

Table 1 The differences on high resolution CO_2 emission estimates by bottom-up approach between this study and previous studies

Table 2 Spatial data used for identifying CO_2 emission sources, and other data used for counting emissions for each sector in Tokyo. Note that several sectors are not consistent with the IPCC definitions. For example, (1) only the LTO cycle emissions were used here for civil aviation, whereas the IPCC sector includes emissions from LTO cycle and cruise; (2) only

907 passenger and cargo ships with round trips to the ports were considered here for the
908 waterborne navigation sector, whereas the IPCC sector covers all water-borne transport, from
909 recreational craft to large ocean-going cargo ships; and (3) two IPCC sectors (manufacturing
910 and commercial sectors) were combined to form the industrial and commercial sector.
911
912 **Table 3** CO_2 emission factors for vehicles by vehicle type and speed (2010), extracted from
913 experimental results [66].
914
915 **Table 4** Annual consumption of fossil fuels, worker numbers, and CO_2 emission factors for
916 workers by category in Tokyo, derived from the 2014 economic census [69] and the energy-
917 balance table for Tokyo (2014) [70].
918
919 **Table 5** CO_2 emission factors for households by occupancy and building type, based on an
920 investigation of residential energy consumption [75].
921
922 **Table 6** CO_2 emission factors for farmland by crop type [78, 79].
923
924 **Table 7** Estimates of annual CO_2 emissions from Tokyo (2014) by sector and source type.
925
926 **Additional file 1**
927 **Table S1** Ownership, facility description, location, and emissions for 106 point-type emission
928 sources (2014). Note: * indicates that the average utilization rate of CAs (2014) from these facilities
929 was extended to all of the waste incineration plants.
930 **Table S2** Municipality names, abbreviations, areas, populations, and emissions for the 62
931 Tokyo municipalities (2014).
932 **Table S3** Parameter settings for the calculation of emissions from vessels [55, 56].
933 Note: GT classes #A: 5–10 t, 10–15 t, 15–20 t, 150–200 t, 350–500 t, 500–1,000 t; #B: 1–70 t,
934 70–500 t, 500–3,000 t; #C: <500 t, 500–1,000 t, 1,000–3,000 t, 3,000–6,000 t, 6,000–10,000 t,
935 10,000–30,000 t, 30,000–60,000 t, 60,000–100,000 t, >100,000 t; #D: <500 t, 500–5,000 t,
936 5,000–10,000 t, >10,000 t.
937 **Table S4** Components of this study and relevant data sources.
938 **Table S5** Differences in emission counting and mapping by source type between EAGrid-
939 Japan and this study.
940 **Table S6** Uncertainties from activity data and emission factors, by sector.

Figures

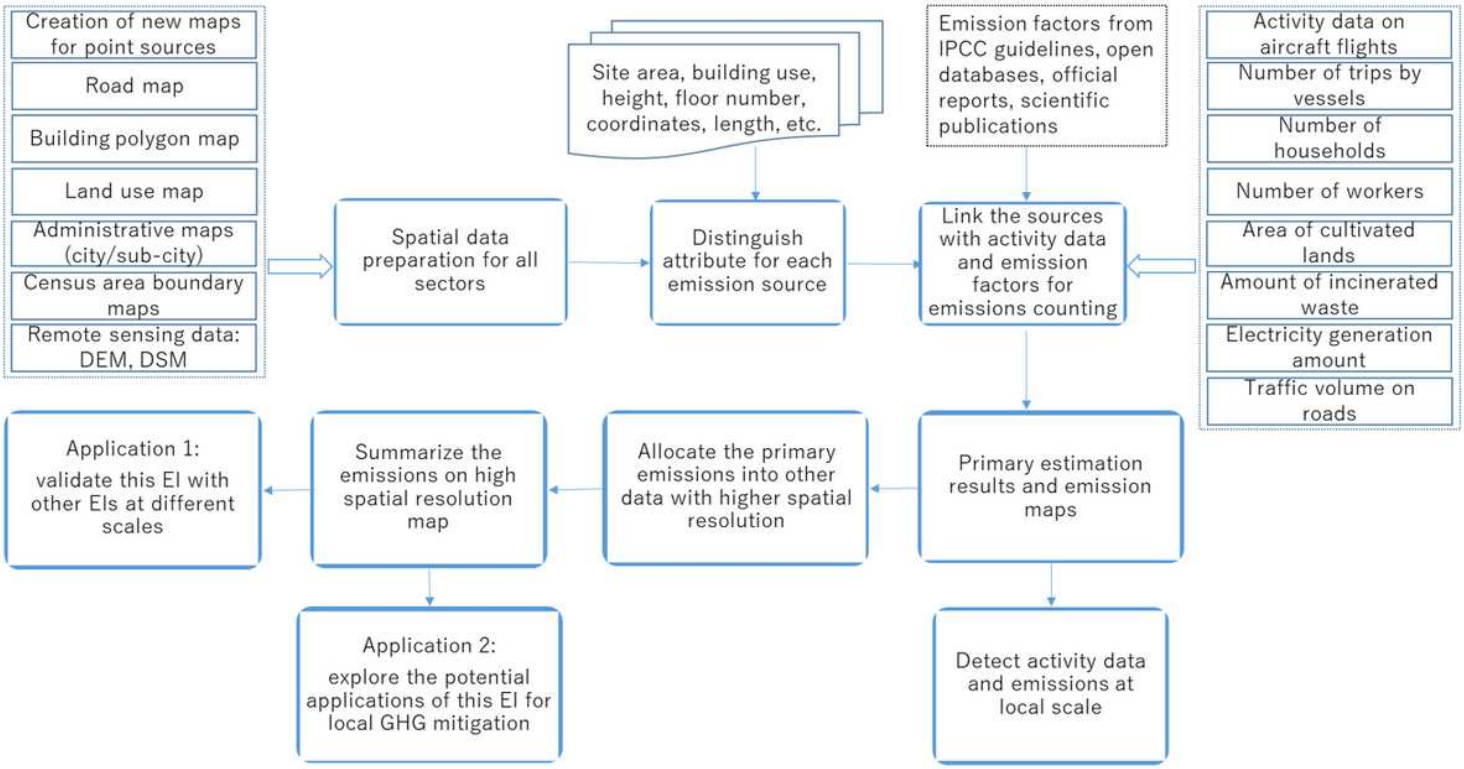

Figure 1

Conceptual framework for emission mapping.

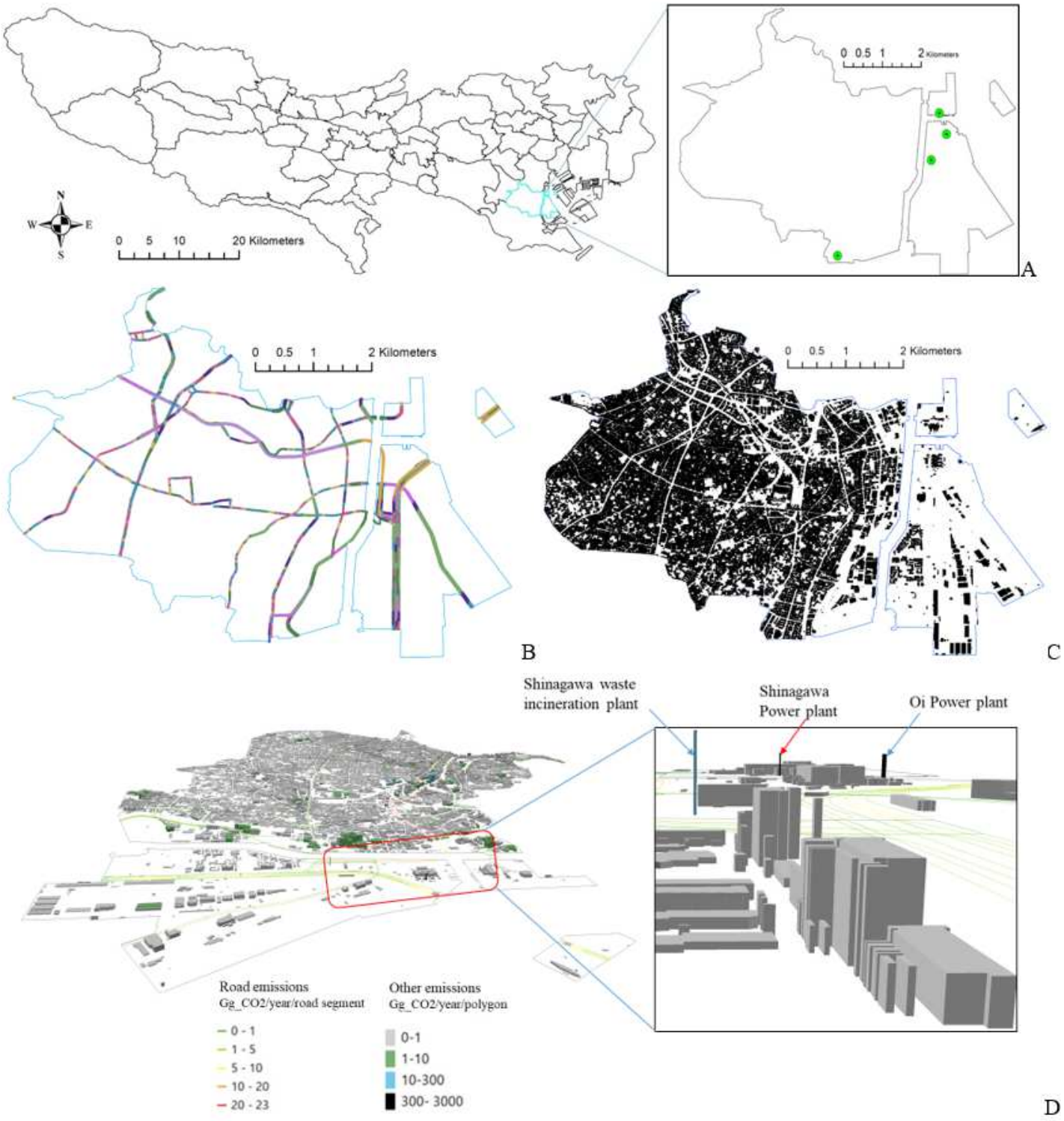

Figure 2

Examples of vector maps for emission sources in SG Ward, Tokyo. (A) Locations of point emission sources. (B) Road segments for line sources. (C) Building polygons for area sources (blue line shows the boundary of the area). (D) 3D emission map for all sources (Gg CO2 yr−1 per road segment for road emissions and Gg CO2 yr−1 per polygon for others).

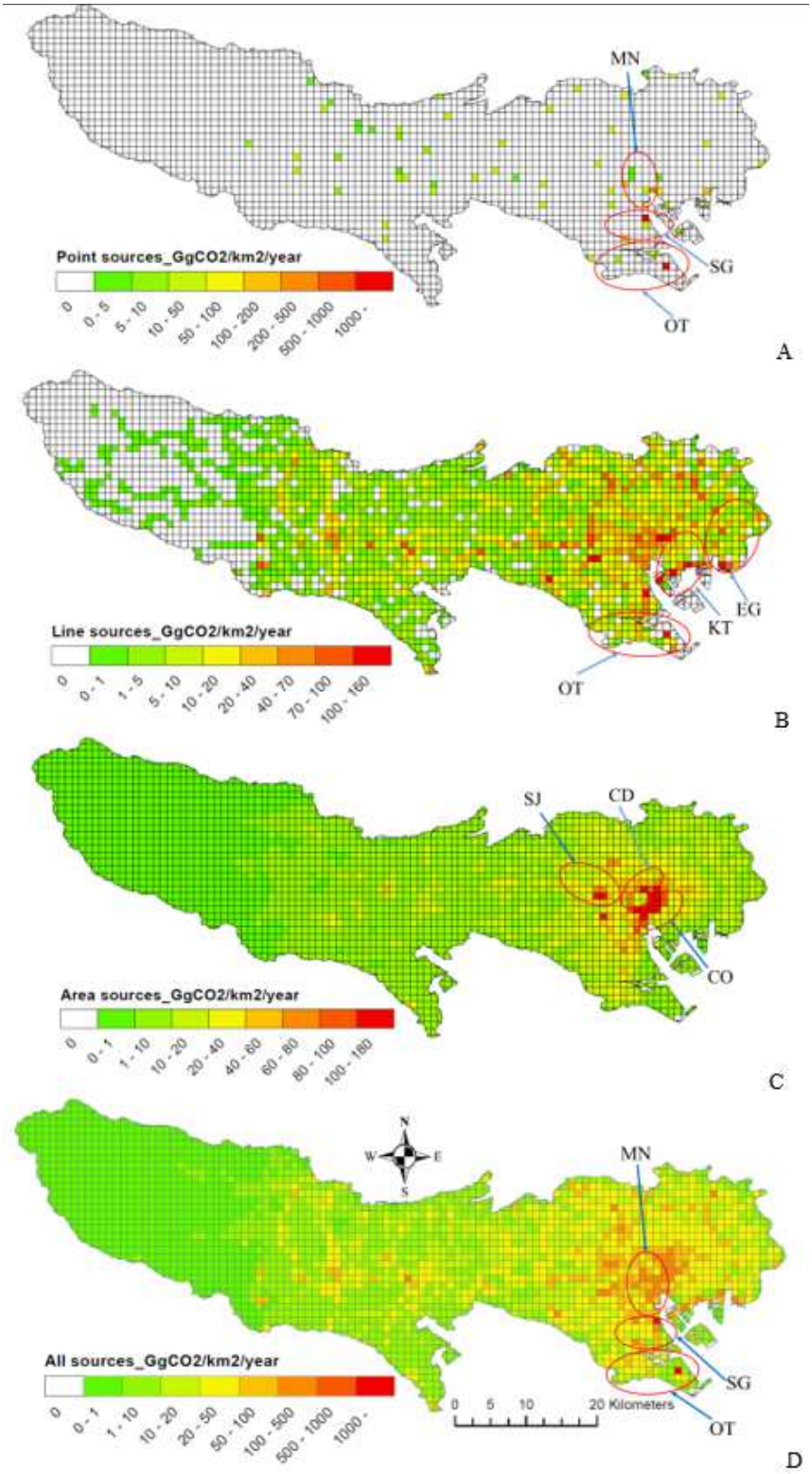

Figure 3

Emission maps with 1 × 1 km mesh for (A) point sources, (B) line sources, (C) area sources, and (D) all sources. Unit: Gg CO2 km−2 yr−1.

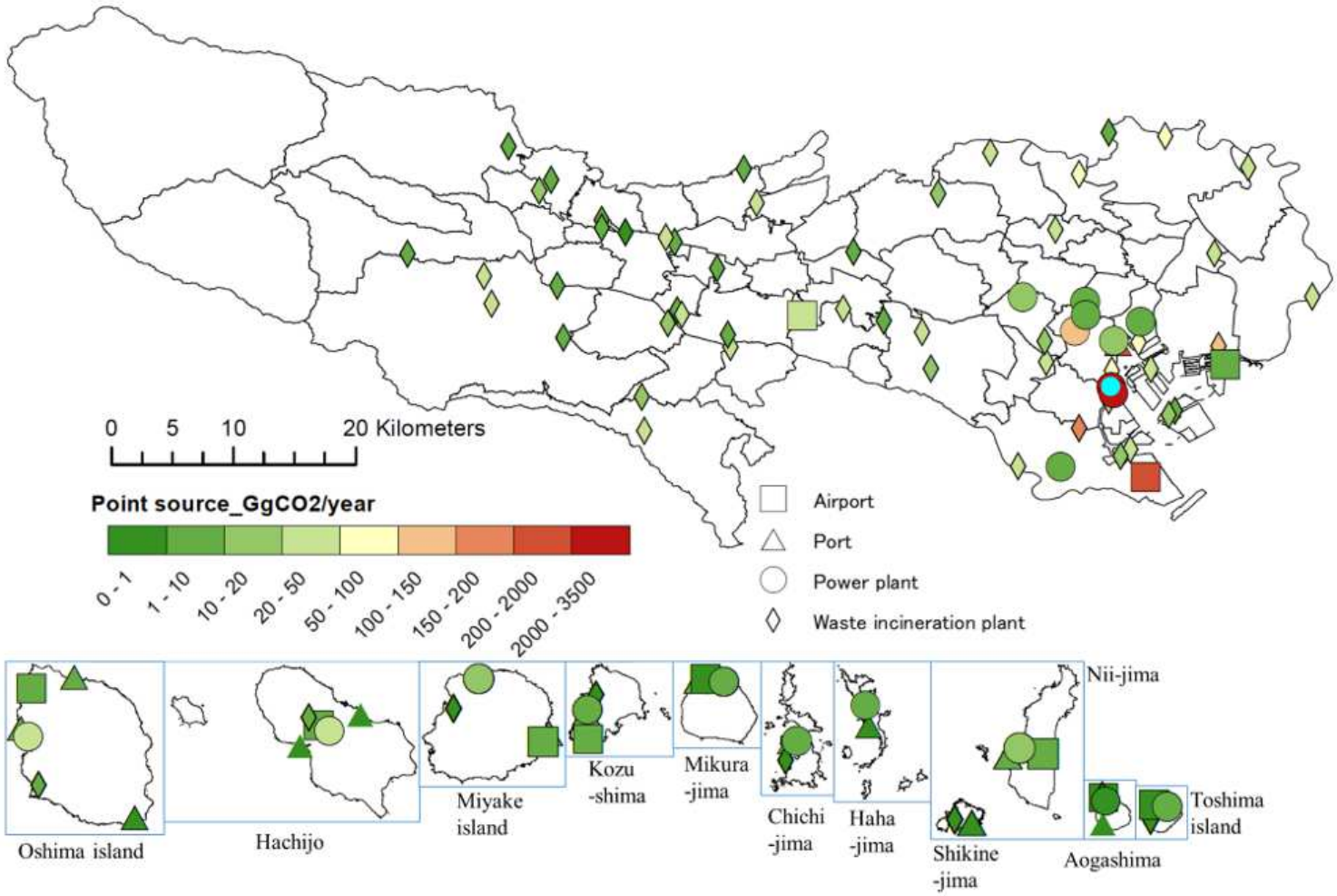

Figure 4

Map of 106 point sources in Tokyo (areas in blue frames indicate islands). The point in cyan indicates the highest emissions at Shinagawa power plant (3,219 Gg CO2 yr−1).

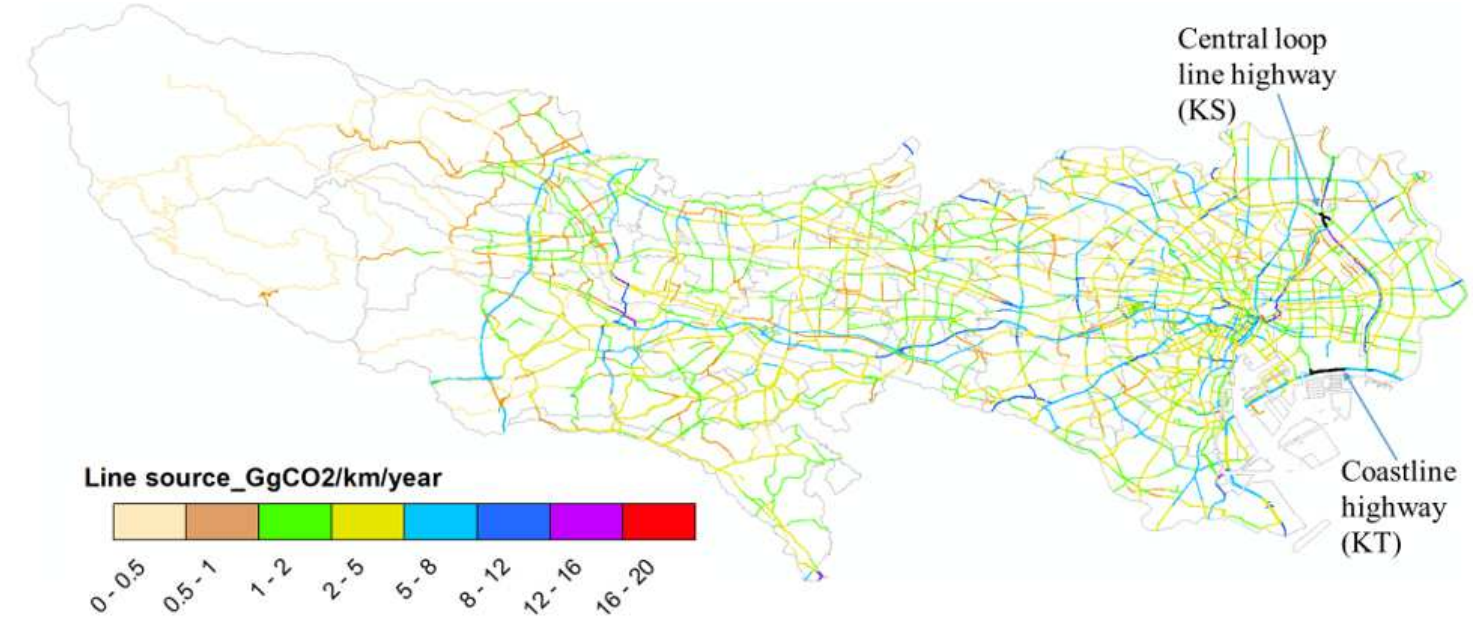

Figure 5

Map of emissions from line sources for each road segment. The 30 road segments with the highest emissions are marked in black. Unit: Gg CO2 km−1 yr−1.

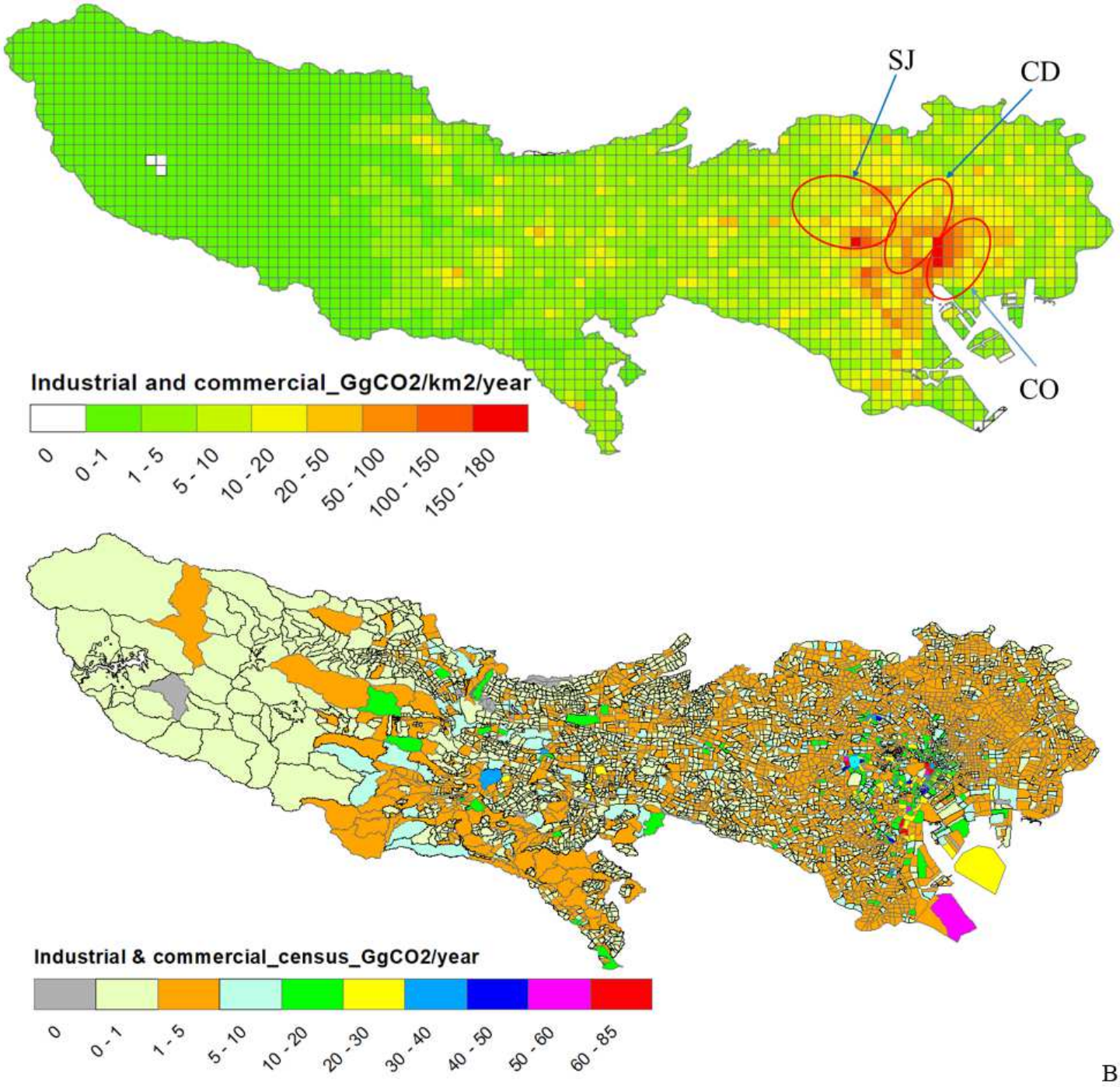

Figure 6

Map of emissions from the industrial and commercial sector with (A) 1 × 1 km mesh, unit: Gg CO2 km−2 yr−1; (B) 5,318 economic census areas, unit: Gg CO2 yr−1. The municipality boundary for the area with the highest annual emissions (up to 82.2 Gg CO2) is marked in cyan.

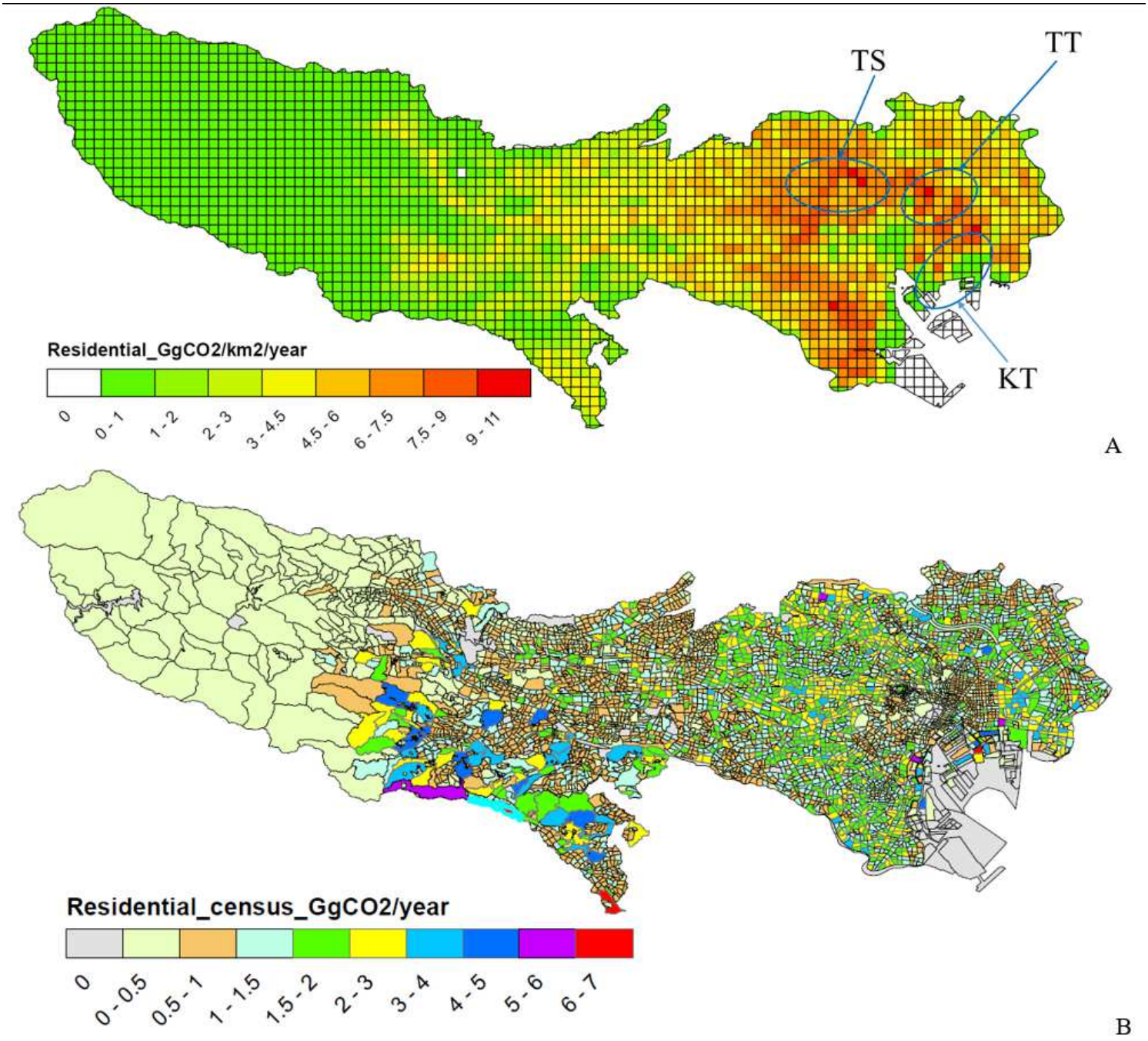

Figure 7

Map of emissions from the residential sector with (A) 1 × 1 km mesh, unit: Gg CO2 km−2 yr−1; (B) 5,578 population census areas, unit: Gg CO2 yr−1. The municipality boundary for the area with the highest annual emissions (up to 6.6 Gg CO2) is marked in cyan.

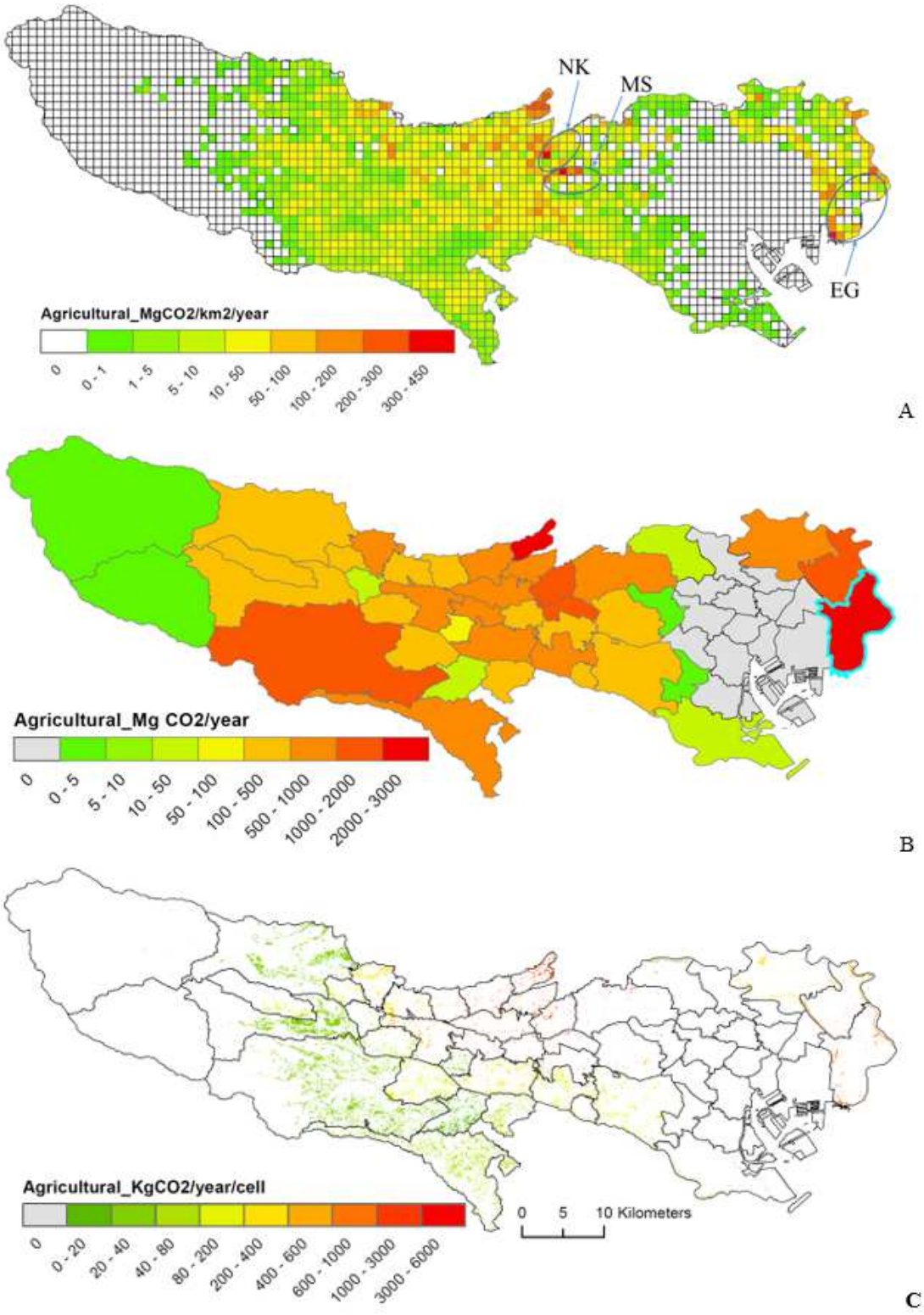

Figure 8

Maps of emissions from the agricultural machine use sector with (A) 1 × 1 km mesh, unit: Mg CO2 km−2 yr-1. (B) 62 municipalities, unit: Mg CO2 yr−1. The area with the highest annual emissions (2,765 Mg CO2 yr−1) is marked in cyan. (C) high-spatial-resolution map on a grid with cell size of 10 × 10 m, unit: Kg CO2 yr−1 per cell.

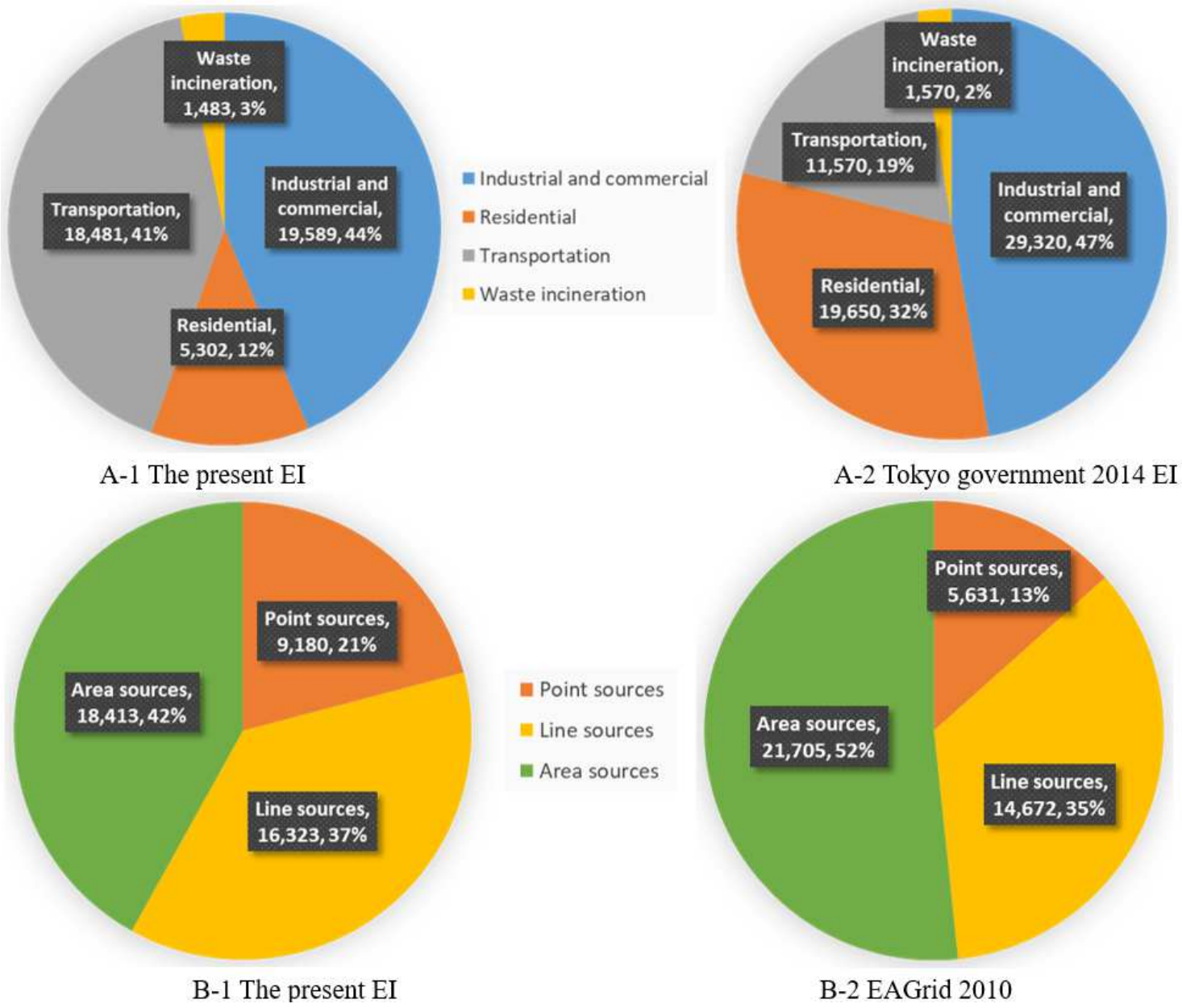

Figure 9

Comparisons on annual CO2 emissions in Tokyo between the present EI (A-1) and Tokyo government 2014 EI (A-2), and between the present EI (B-1) and EAGrid-Japan 2010 (B-2). Unit: Gg CO2. Note: In A-1, the industrial and commercial category includes emissions from the industrial and commercial sector and the electricity generation sector. The transportation category includes emissions from the road transportation, civil aviation, and waterborne navigation sectors. In A-2, the transportation category includes emissions from the railway, road transportation, civil aviation, and waterborne navigation sectors. In B-2, point sources include power plants, waste incineration plants, vessels, and aircrafts. Line sources refer to road transportation. Area sources include residential and commercial combustion equipment, factory and building boilers, off-road transportation, open burning, and facilities without identified locations.

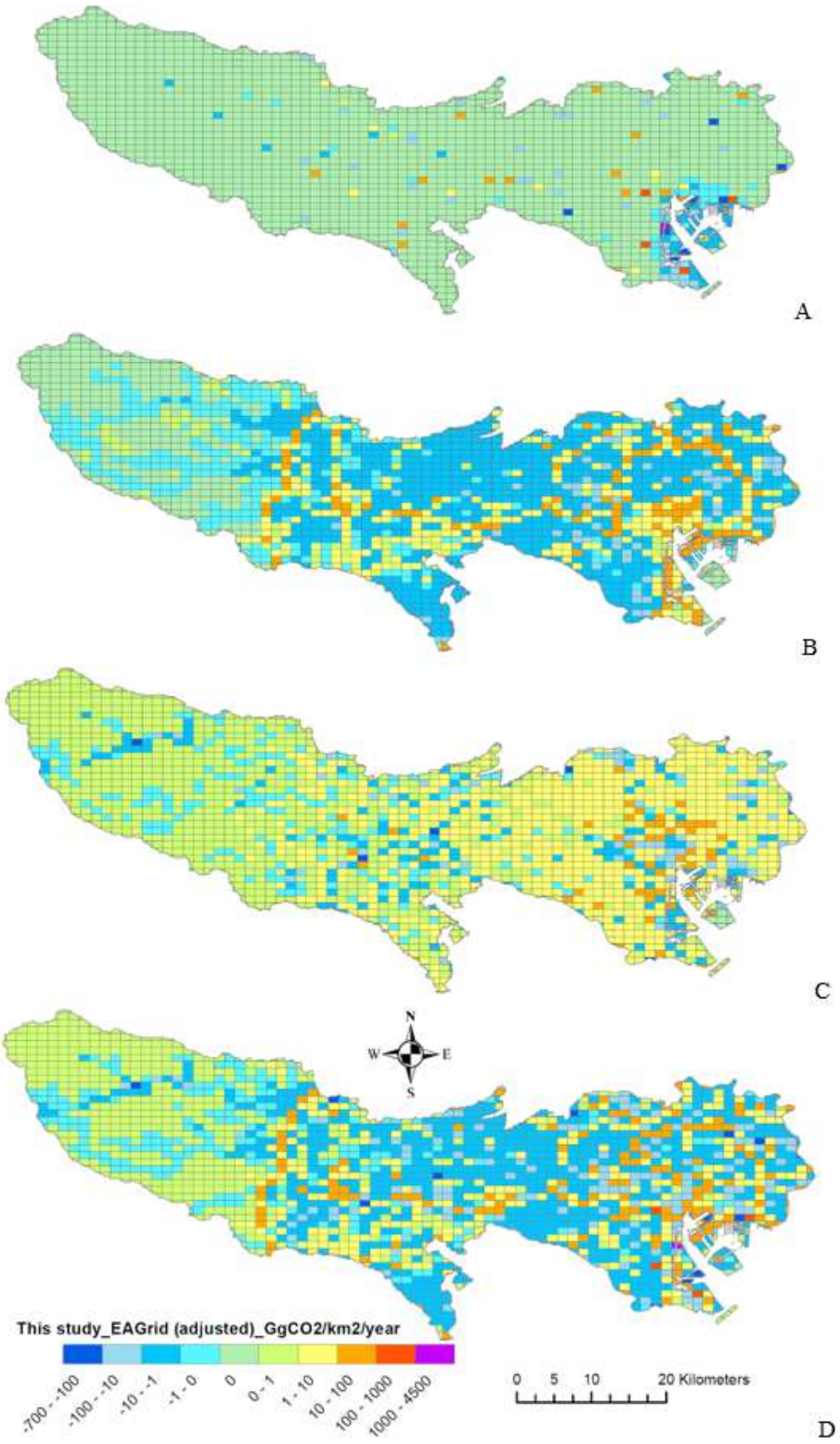

Figure 10

Differences in emissions between the present EI and 2010 EAGrid-Japan EI at a resolution of 1 X 1 km for: (A) point sources, (B) line sources, (C) area sources, and (D) all sources. Unit: Gg CO2 km−2 yr−1. (Difference = emissions from the present EI – 2010 EAGrid-Japan EI, after adjustment of EAGrid emissions, as described in the text.).

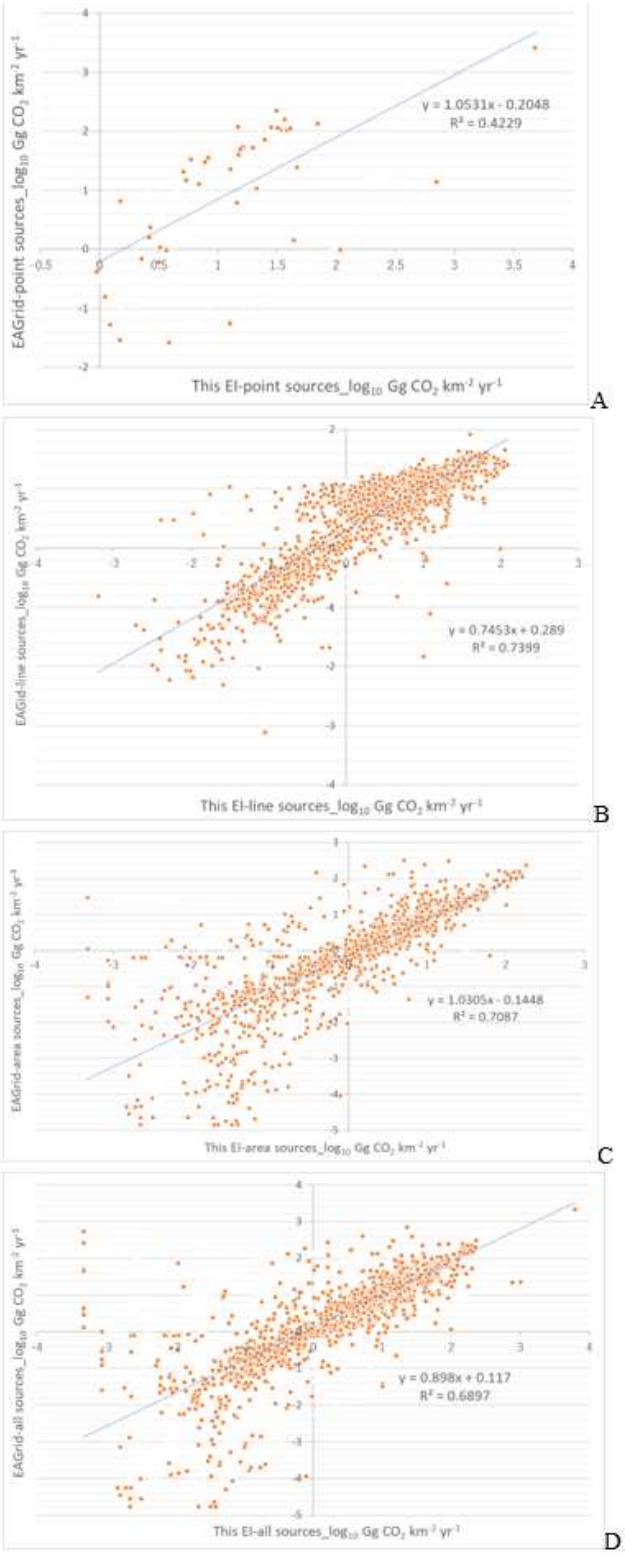

Figure 11

Scatter plots of gridded emissions by source types between the present EI and EAGrid for: (A) point sources, (B) line sources, (C) area sources, and (D) all sources. Unit: log10 Gg CO2 km−2 yr−1.

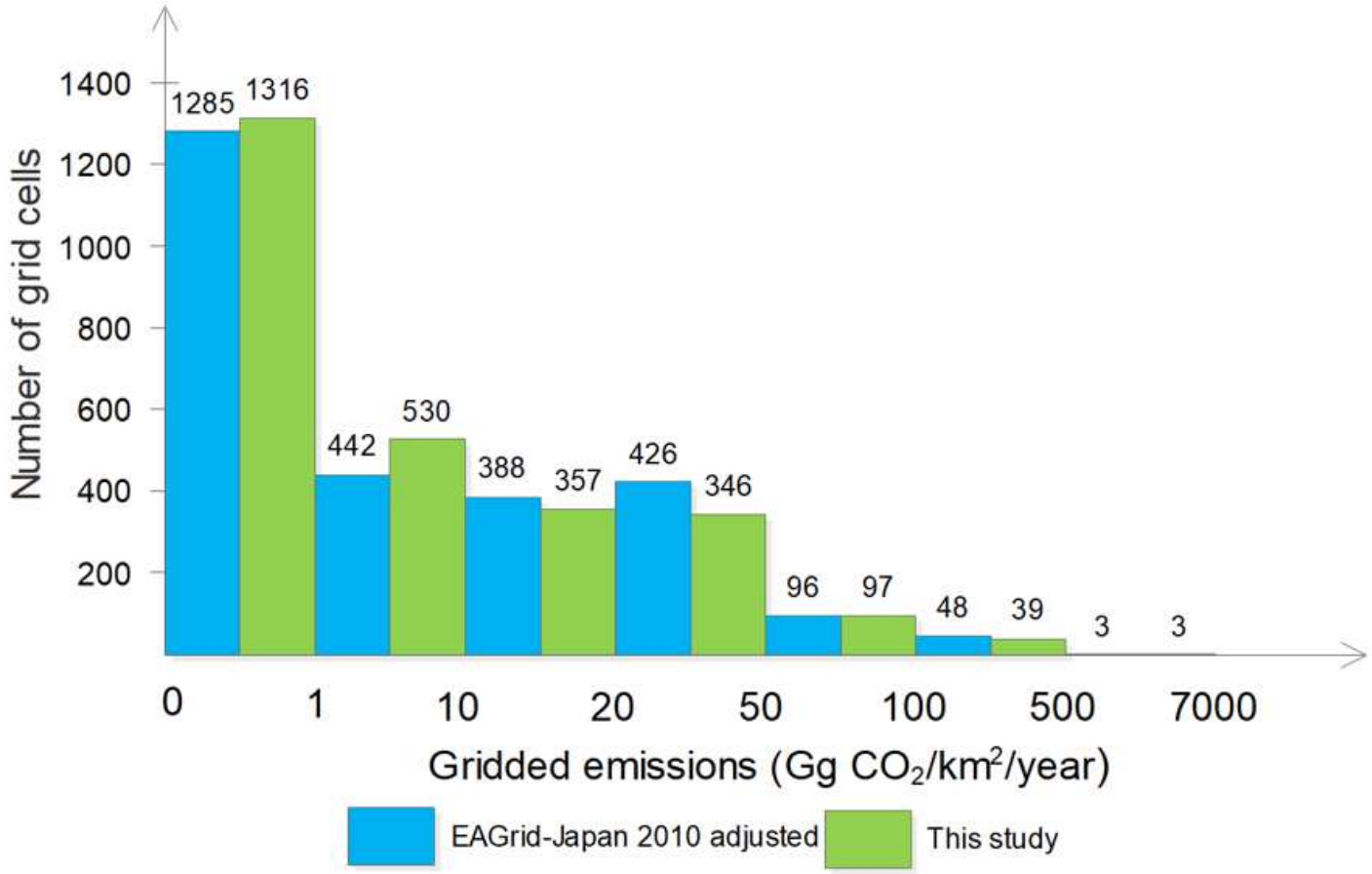

Fig. 12 Frequency distribution of gridded emissions (Gg CO_2 km^{-2} yr^{-1}) for this study (green) and EAGrid-Japan 2010 adjusted (blue). n = 2,688

Figure 12

Frequency distribution of gridded emissions (Gg CO2 km−2 yr−1) for this study (green) and EAGrid-Japan 2010 adjusted (blue). n = 2,688.

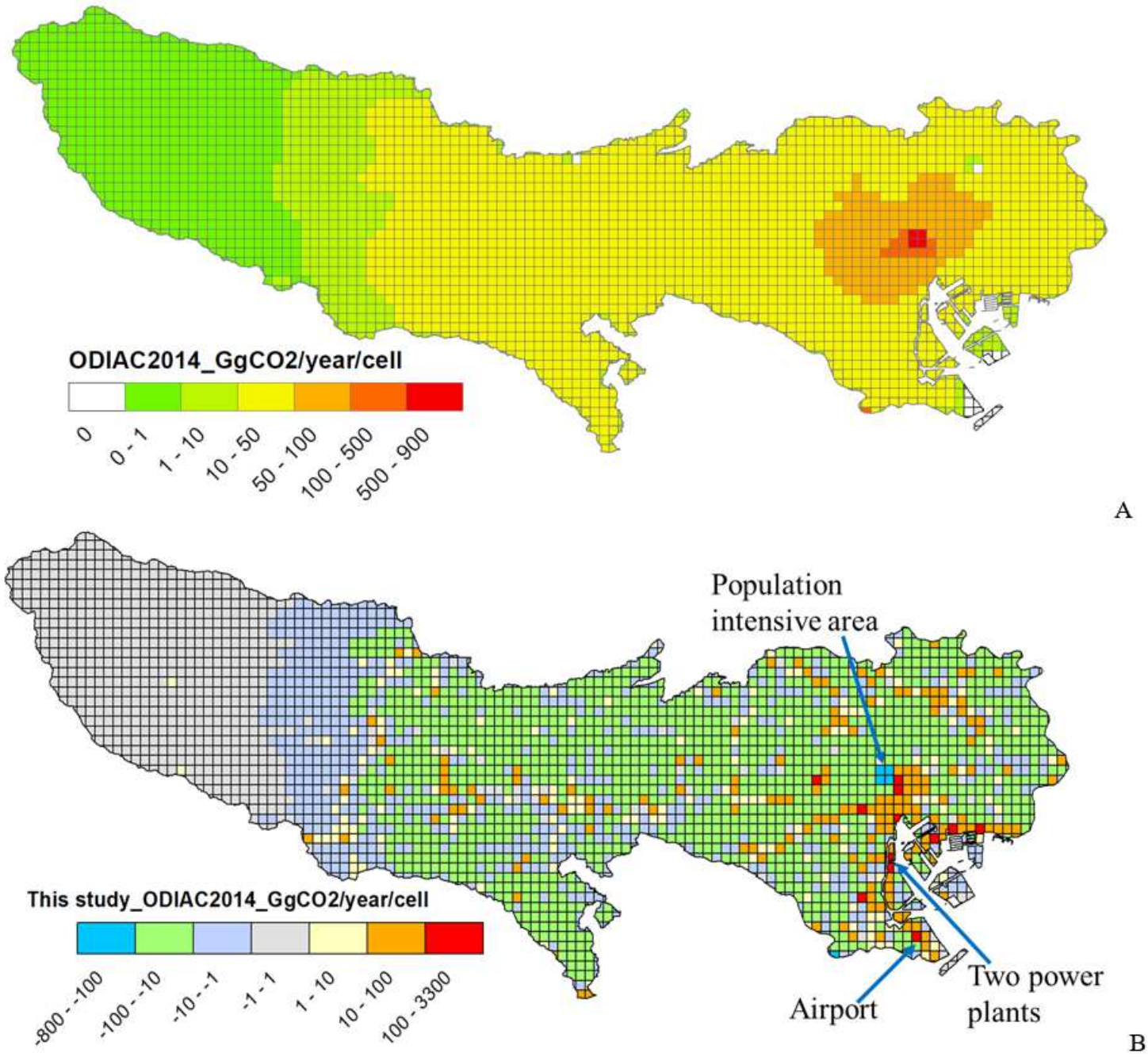

Figure 13

Emission maps with a 30 × 30 arcsec mesh size for (A) ODIAC 2014 clipped for the Tokyo domain, (B) gridded emission differences between this study and ODIAC 2014 clipped for the Tokyo domain (Difference = emissions from the present EI minus ODIAC 2014). Unit: Gg CO2 yr−1 cell−1.

Supplementary Files

This is a list of supplementary files associated with this preprint. Click to download.

- Supplement.docx